JVI
Journals.ASM.org

Simultaneous Treatment of Human Bronchial Epithelial Cells with Serine and Cysteine Protease Inhibitors Prevents Severe Acute Respiratory Syndrome Coronavirus Entry

Miyuki Kawase,[a] Kazuya Shirato,[a] Lia van der Hoek,[c] Fumihiro Taguchi,[b] and Shutoku Matsuyama[a]

Department of Virology III, National Institute of Infectious Diseases, Murayama Branch, Gakuen Musashi-Murayama, Tokyo, Japan[a]; Faculty of Veterinary Medicine, Nippon Veterinary and Life Science University, Kyonan-cho, Musashino, Tokyo, Japan[b]; and Department of Medical Microbiology, University of Amsterdam, Faculty of Earth and Life Sciences, Amsterdam, The Netherlands[c]

The type II transmembrane protease TMPRSS2 activates the spike (S) protein of severe acute respiratory syndrome coronavirus (SARS-CoV) on the cell surface following receptor binding during viral entry into cells. In the absence of TMPRSS2, SARS-CoV achieves cell entry via an endosomal pathway in which cathepsin L may play an important role, i.e., the activation of spike protein fusogenicity. This study shows that a commercial serine protease inhibitor (camostat) partially blocked infection by SARS-CoV and human coronavirus NL63 (HCoV-NL63) in HeLa cells expressing the receptor angiotensin-converting enzyme 2 (ACE2) and TMPRSS2. Simultaneous treatment of the cells with camostat and EST [(23,25)*trans*-epoxysuccinyl-L-leucylamindo-3-methylbutane ethyl ester], a cathepsin inhibitor, efficiently prevented both cell entry and the multistep growth of SARS-CoV in human Calu-3 airway epithelial cells. This efficient inhibition could be attributed to the dual blockade of entry from the cell surface and through the endosomal pathway. These observations suggest camostat as a candidate antiviral drug to prevent or depress TMPRSS2-dependent infection by SARS-CoV.

Both the severe acute respiratory syndrome coronavirus (SARS-CoV) and human coronavirus NL63 (HCoV-NL63) utilize angiotensin-converting enzyme 2 (ACE2) as an essential receptor for cell entry. Although ACE2 is present in the vesicular endothelial cells of all organs, these viruses are highly pathogenic only in the lungs. Furthermore, for SARS-CoV, the distribution of ACE2 does not strictly correlate with viral cell tropism. While ACE2 expression in the lungs has been shown in both type I and type II pneumocytes, the cell tropism of SARS-CoV has only been shown in type I pneumocytes during the early stages of infection (13, 19, 32). Therefore, it is predicted that both the receptor and a cofactor are required for viral entry into pneumocytes. Host cellular proteases play a critical role in the process of SARS-CoV entry into cells. Specifically, cathepsin L, trypsin, elastase, TMPRSS11a, hypoxanthine-aminopterin-thymidine (HAT), and TMPRSS2 activate the SARS-CoV spike (S) protein, which is a prerequisite for the fusion of viral and host cell membranes during viral entry (1, 2, 6, 15–17, 19, 20, 23, 27–30).

TMPRSS2 is expressed on the epithelial cells of human lungs (15, 19, 24), and its ability to activate viral glycoproteins has also been reported for influenza A virus, metapneumovirus, and porcine epidemic diarrhea virus (PEDV) (3–5, 7–12, 25, 26). The difference between these viruses and SARS-CoV occurs during the virus replication stage, during which viral glycoproteins are cleaved by proteases. The protease makes a simple cut in the glycoprotein during the maturation of the influenza A virus and metapneumovirus, in a manner similar to that made by furin. In the case of PEDV, TMPRSS2 enhances the release of viral particles into the culture fluid (25). In contrast, SARS-CoV spike (S) protein is predicted to be cleaved by TMPRSS2 following receptor binding for virus cell entry, which expected from the study for the S protein activation by trypsin (29). Recently, Bertram reported that HAT activates SARS-CoV S protein both in *cis* and in *trans* for cell-cell fusion, whereas TMPRSS2 activates S protein for cell-cell and virus-cell fusion in *trans* only (4). The multiple protease cleavage sites within the SARS-S protein are reportedly located closer to the C-terminal region than the putative cleavage sites of other coronaviruses (1, 4, 19, 27, 33); however, the site cleaved by TMPRSS2 for S protein activation has yet to be precisely identified.

Protease availability appears to determine the route of cell entry of SARS-CoV. In the absence of proteases at the cell surface, SARS-CoV enters cells by an endosomal pathway and the S protein is fusogenically activated by cathepsin L, thereby allowing fusion of the viral and endosome membranes (17, 19, 30). In contrast, in the presence of proteases such as trypsin, elastase, and TMPRSS2, which induce envelope-plasma membrane fusion, SARS-CoV enters the cell cytoplasm directly from the cell surface (19, 27). Despite these observations, the precise mechanisms by which SARS-CoV penetrates the cell surface are currently unknown; however, it is possible that entry is via an early endosome, similar to that reported for HIV (22). Based on the importance of TMPRSS2 for S protein activation, the aim of the present study was to identify an inhibitor of TMPRSS2 from commercial drugs that could prevent SARS-CoV and HCoV-NL63 infection in cell culture as well as in humans.

MATERIALS AND METHODS

Cells and viruses. HeLa cells expressing both ACE2 and TMPRSS2 (HeLa-ACE2-TMPRSS2) were prepared by cotransfecting HeLa229 cells

Received 17 January 2012 Accepted 30 March 2012
Published ahead of print 11 April 2012
Address correspondence to Shutoku Matsuyama, matuyama@nih.go.jp.

doi:10.1128/JVI.00094-12

with a pTargeT plasmid (Promega, Madison, WI) harboring the human ACE2 gene and a pcDNA plasmid harboring the human TMPRSS2 gene, followed by selection in a medium containing G418. HeLa229 cells expressing only ACE2 (HeLa-ACE2) were established by transfecting the cells with a plasmid carrying the ACE2 gene. The cells were grown and maintained in Dulbecco's modified Eagle's medium (DMEM; Nissui, Tokyo, Japan) supplemented with 5% fetal bovine serum (Sigma, St. Louis, MO). Human bronchial epithelial Calu-3 cells were grown in modified Eagle's medium (MEM) supplemented with 10% fetal calf serum (FCS) as recommended by the American Tissue Culture Collection (ATCC). The SARS-CoV Frankfurt 1 strain was propagated and assayed using Vero E6 cells, as previously described (20). The HCoV-NL63 strain was propagated and assayed using LLC-MK2 cells as previously described (16). Pseudotyped vesicular stomatitis virus (VSV) expressing green fluorescent protein (GFP) and harboring SARS-CoV S protein or VSV-G protein was prepared as previously described (14). The production of a VSV pseudotype bearing the NL63-S protein is described below.

Generation of VSV pseudotyped with NL63-S protein. The S protein of SARS-CoV with a C-terminal 19-amino-acid deletion has been reported to efficiently incorporate into VSV-based pseudotyped virus (14). Therefore, we tried to generate VSV-based pseudotyped virus bearing NL63-S protein using this C-terminally truncated S protein. The cDNA fragment of the full-size S protein, or the S protein with a ≥19-amino-acid truncation from the C terminus, was amplified by reverse transcription-PCR (RT-PCR) and cloned into the mammalian expression vector pTargeT. In addition, the TransIT-293 transfection reagent (Mirus Bio, Madison, WI) was used to transfect 293T/17 cells, obtained from the ATCC (CRL-11268) with the expression plasmid, followed by incubation at 37°C for 30 to 36 h. These cells were then infected with VSV[Delta]G-G, which encodes the VSV-G protein, but with replacement of the gene by a GFP gene (kindly provided by M. A. Whitt, GTx, Inc., Memphis, TN) and were incubated at 37°C for 1 h. After four washes with phosphate-buffered saline (PBS), the cells were further incubated at 37°C for 24 h. The culture fluid was collected, centrifuged at 1,000 rpm for 5 min at 4°C, aliquoted into cryotubes, and stored at −80°C until use. The controls were VSV-pseudotyped viruses bearing VSV-G proteins, generated as previously reported (14). The infectivity of the pseudotyped viruses was determined by counting the number of GFP-positive cells and expressed as infectious units (IU). Finally, we chose the pseudotyped NL63-S (with a 24-amino-acid truncation) as it efficiently infected HeLa-ACE2, but not HeLa, cells.

Inhibitors. The following inhibitors were used in this study: benzamidine hydrochloride (A1380; AppliChem), aprotinin (A213; AppliChem), tosyl lysyl chloromethyl ketone (TLCK) (BML-P1121; Enzo Life Sciences), gabexate mesylate (G2417; Sigma), EST [(23,25)*trans*-epoxysuccinyl-L-leucylamindo-3-methylbutane ethyl ester] (330005; Calbiochem), bafilomycin A1 (B1793; Sigma), MDL28170 (M6690; Sigma), cathepsin L inhibitor III (219427; Calbiochem), leupeptin (11017101001; Roche), cytochalasin D (C8273; Sigma), and camostat mesylate (3193; Tocris Bioscience). The concentrations are specified in the figure legends.

Pseudotyped virus entry assay. HeLa-ACE2 or HeLa-ACE2-TMPRSS2 cells in 96-well plates were treated with growth medium containing the above-described inhibitors for 30 min at 37°C. Approximately 10^5 IU of virus was then used to infect 10^5 cells in the presence of the inhibitors. The cells were then cultured at 37°C for 20 h. GFP-positive cells were photographed under a fluorescence microscope (Keyence Corporation, Osaka, Japan) and counted using image measurement and analysis software (VH-H1A5 version 2.6; Keyence). The inhibitory effect was calculated by counting the number of GFP-positive cells, as previously described (18).

Quantification of transcripts. The mRNAs for ACE2, HAT, and TMPRSS2 were compared in Calu-3 cells and human lung cells. Human lung cell total RNA, isolated from three male and three female Caucasians ages 32 to 61 years, was purchased from Clontech (636524). In addition, cellular Calu-3 RNA was isolated using the Isogen reagent (Nippon Gene) according to the manufacturer's protocol. The TMPRSS2 mRNA fragment was amplified with the oligonucleotide pair 5′-CTCTACGGACCAAACTTCATC-3′ and 5′-CCACTATTCCTTGGCTAGAGTAA-3′, and hybridization was detected with the probes 5′-TCAGAGGAAGTCCTGGCACCCTGTGT G-3′ (3′-fluorescein isothiocyanate [FITC] labeled) and 5′-CAAGACGA CTGGAACGAGAACTACGGGC-3′ (5′-LCRed640 labeled). The HAT mRNA fragment was amplified using the oligonucleotide pair 5′-CTTGT GAGACTTGAGAACAGTG-3′ and 5′-ACCTGTCCTTGCCTTAGC-3′, and hybridization was detected with the probes 5′-GCCAGCATATTCT TGAGCGCCCCA-3′ (3′-FITC labeled) and 5′-CCTGTTACATAAGCA GTAGAGCCAGGTGGAAT-3′ (5′-LCRed640 labeled). The amount of ACE2 mRNA was estimated using the oligonucleotide pair 5′-CCGTAT CAATGATGCTTTCCG-3′ and 5′-CAGTGAAGATCAGGATGACAAT G-3′, and hybridization was detected with the probes 5′-ACCTCCTAAC CAGCCCCCTGTTTCCATA-3′ (3′-FITC labeled) and 5′-GGCTGATTG TTTTTGGAGTTGTGATGGGAG-3′ (5′-LCRed640 labeled). PCR analysis was performed in a LightCycler instrument (Roche Diagnostics). The mRNA copy number was calculated based on a calibration line obtained by 10-fold stepwise dilution of plasmid DNA.

Knockdown of TMPRSS2 and HAT. Calu-3 cells with knocked-down human TMPRSS2, HAT, or a nontargeting control were generated using the respective small interfering RNA (siRNA) oligonucleotides (E-006048-00, E-005894-00, and D-001910-10-05; Dharmacon) in a transient transfection carried out according to the manufacturer's protocol. Knockdown of human TMPRSS2 or HAT was estimated by real-time PCR.

Authentic SARS-CoV entry assay. HeLa-ACE2, HeLa-ACE2-TMPRSS2, and Calu-3 cells in 96-well plates were treated with DMEM containing inhibitors at 37°C for 30 min. Approximately 10^3 PFU of SARS-CoV (see Fig. 2B), 10^1 PFU of HCoV-NL63 (Fig. 2B), and 10^6 PFU of SARS-CoV (see Fig. 9 and 10) in DMEM plus inhibitors were used to infect 10^5 cells, which were then cultured at 37°C for 5 h. Cellular RNA was isolated by the addition of 200 μl of Isogen reagent (Nippon Gene). Real-time PCR was performed to estimate the amount of newly synthesized mRNA9 of SARS-CoV, as previously described (19). The mRNA9 for SARS-CoV was amplified using the oligonucleotide pair 5′-CTCGATCTCTTGTAGATCTG-3′ and 5′-TCTAAGTTCCTCCTTGCCAT-3′, and hybridization was detected with the probes 5′-ACCAGAATGGAGGACGCAATGGGGCAAG-3′ (3′-FITC labeled) and 5′-CCAAAACAGCGCCGACCCCAAGGTTTAC-3′ (5′-LCRed640 labeled). The mRNA9 of HCoV-NL63 was amplified using the oligonucleotide pair 5′-TTAGACTTTGTGTCTACTC-3′ and 5′-TA CGCCAACGCTCTTGAAC-3′, and hybridization was detected with the probes 5′-TTATTACCCTTACCAATAGGGACAAGATTCCTGGG-3′ (3′-FITC labeled) and 5′-ATGACCCTATATGGTGCCTTATCAGAACT AACCAAAAG-3′ (5′-LCRed640 labeled). PCR analysis was performed in a LightCycler instrument (Roche Diagnostics). Viral mRNA levels were normalized to the expression levels of the cellular housekeeping gene coding for glyceraldehyde-3-phosphate dehydrogenase (GAPDH).

Multistep growth of authentic SARS-CoV. Subconfluent Calu-3 cells (10^6 cells) were inoculated into 24-well plates with 10^4 PFU of SARS-CoV in DMEM and incubated for 2 h at 37°C. Residual virus was then removed, and the medium was replaced with fresh medium with 10 μM cathepsin inhibitor EST, 10 μM camostat, or both. Cellular RNA was isolated from the cells from four wells every 24 h for 6 days by adding 400 μl of Isogen reagent. The growth kinetics of SARS-CoV were estimated by measuring viral mRNA9 using real-time PCR as previously described (20).

RESULTS

Cell entry of pseudotyped viruses in the presence of exogenous trypsin or TMPRSS2. A nonenzymatic cell dissociation solution (C5914; Sigma), rather than trypsin, was used for passaging cells, as exogenous trypsin may lead to an overestimation of the level of human coronavirus infection. Protease-dependent cell entry of coronaviruses into HeLa cells stably expressing human ACE2 was estimated as follows. First, VSV pseudotypes bearing SARS-S, NL63-S, or VSV-G were treated with trypsin (TLCK treated) (T-8802; Sigma) for 5 min at 37°C and then inoculated into the cells

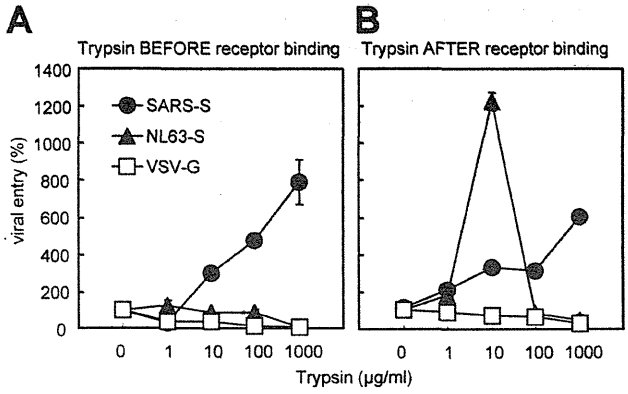

FIG 1 Enhancement of protease-mediated viral entry into cells. (A) Pseudotyped viruses bearing SARS-S, NL63-S, or VSV-G were incubated with serially diluted trypsin for 5 min at 37°C, followed by inoculation onto HeLa-ACE2 cells for 30 min on ice. (B) Pseudotyped viruses were first adsorbed onto HeLa-ACE2 cells for 30 min on ice, followed by the addition of serial dilutions of trypsin to cells and incubation for a further 5 min at 37°C. The medium was then changed, and the cells were incubated for 20 h at 37°C. Infectivity was quantified by counting GFP-positive cells. The results are presented as the percentage of infected cells (at least 50 GFP-positive cells were counted). Error bars indicate the standard deviations (SD) of the means from four independent wells.

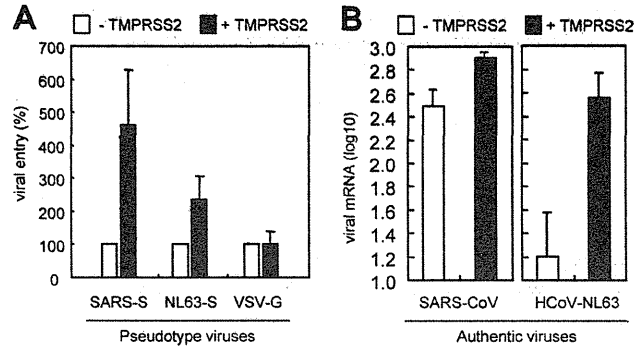

FIG 2 Effect of TMPRSS2 on virus entry into cells. (A) Pseudotyped viruses were inoculated onto HeLa-ACE2 (white bars) and HeLa-ACE2-TMPRSS2 (black bars) cells. Infectivity was quantified by counting GFP-positive cells 20 h after viral inoculation. The results are presented as the percentage of infected HeLa-ACE2 cells (at least 50 GFP-positive cells were counted). Error bars indicate the SD of the means from eight independent samples. (B). Authentic SARS-CoV and HCoV-NL63 were inoculated onto HeLa-ACE2 (white bars) and HeLa-ACE2-TMPRSS2 (black bars) cells. Infectivity was quantified by real-time PCR to measure the viral mRNA9 of these viruses. Error bars indicate the SD of the means from four independent samples.

for 30 min on ice. The medium was then changed, and the cells were incubated for 20 h at 37°C. Infection by pseudotyped virus was monitored by GFP expression. Figure 1A shows that whereas a high concentration of trypsin (1 mg/ml) inactivated pseudotyped virus bearing NL63-S, it activated SARS-S-bearing virus. Thus, unlike NL63-S, SARS-S is resistant to trypsin and may be activated by cleavage after receptor binding. Second, pseudotyped viruses were adsorbed onto cells for 30 min on ice, followed by the addition of trypsin for 5 min at 37°C. Pseudotyped SARS-S on the cell surface was activated by trypsin in a concentration-dependent manner, whereas strong activation of NL63-S occurred only at a concentration of 10 μg/ml (Fig. 1B). Third, we evaluated whether cell entry by the viruses was enhanced by TMPRSS2. HeLa-ACE2 or HeLa-ACE2-TMPRSS2 cells were infected with pseudotyped viruses. Figure 2A shows the averages derived from the control data in this study, i.e., pseudotyped virus infection in the absence of inhibitors. Pseudotyped SARS-S entry increased 5-fold in the presence of TMPRSS2, and pseudotyped NL63-S entry increased by 2.5-fold. VSV infection was not affected by TMPRSS2. To facilitate comparison of the decrease in infection due to inhibitors between the experiments, these control data (pseudotyped virus entry into HeLa-ACE2 and HeLa-ACE2-TMPRSS2 cells in the absence of inhibitors) were assumed to represent 100% viral entry in the following figures. Furthermore, cell entry by authentic SARS-CoV and HCoV-NL63 was also tested, and real-time PCR was used to detect the newly synthesized viral mRNA9. Figure 2B shows that SARS-CoV entry increased 2.6-fold and HCoV-NL63 entry increased 23-fold in the presence of TMPRSS2.

Effects of serine protease inhibitors on viral entry. The specific inhibitory effects of chemicals on TMPRSS2 were examined by observing their ability to suppress cell entry by pseudotyped virus. HeLa-ACE2 or HeLa-ACE2-TMPRSS2 cells were treated with benzamidine, aprotinin, gabexate, camostat, and TLCK for 30 min and then inoculated with pseudotyped viruses in the continued presence of these inhibitors. Figure 3A shows that only camostat blocked the entry of pseudotyped SARS-S and NL63-S into TMPRSS2-expressing cells. Suppression by TLCK was not restricted to TMPRSS2-expressing cells since TLCK inhibited pseudotyped SARS-S and NL63-S in both HeLa-ACE2 and HeLa-ACE2-TMPRSS2 cells, indicating that TLCK targets not only TMPRSS2 but cathepsins as well. The concentration-dependent effect of camostat on viral entry was compared with that of its analog, gabexate, in Fig. 3B. Camostat-mediated suppression of SARS-S entry never exceeded 65%, even in the presence of a high concentration of the drug (100 μM), indicating that, despite the presence of TMPRSS2, 35% of the viruses utilized endosomal cathepsins for cell entry. In contrast, in the absence of TMPRSS2, camostat had insignificant effects on pseudotyped virus entry. Similar results were seen for NL63-S.

To confirm the effects of camostat on S protein activation, we examined the inhibition of syncytium formation. Plasmids pKS/SARS-S and pTarget/NL63-S were transfected into HeLa-ACE2-TMPRSS2 cells with pEGFP plasmids to visualize transfected cells. These cells were then cultured in the presence of serially diluted camostat. After 22 h, syncytia were observed in SARS-S- and NL63-S-transfected cells, but their formation was inhibited by camostat (Fig. 4A). Nuclei were stained with 4′,6-diamidino-2-phenylindole (DAPI), and the extent of syncytium formation was quantified by counting the number of nuclei in the fused cells (eight syncytia). Syncytium formation was moderately inhibited by camostat at concentrations of 0.1 μM and 1 μM and completely inhibited at a concentration of 10 μM (Fig. 4B). These results indicated that camostat prevents the activation of S protein at the cell surface.

Effects of cathepsin inhibitors on viral entry. SARS-CoV utilizes endosomal cathepsin L, and infection is blocked by cathepsin L inhibitors (30). In contrast, HCoV-NL63 does not utilize endosomal cathepsin L (16). EST, a broad inhibitor of cysteine proteases, including cathepsins, is also unable to block infection by NL63 (16). Here, we examined the inhibition of viral entry in the presence of EST, MDL, cathepsin L inhibitor III (LIII), and leupeptin (Leu). Two other inhibitors, bafilomycin A1, which blocks

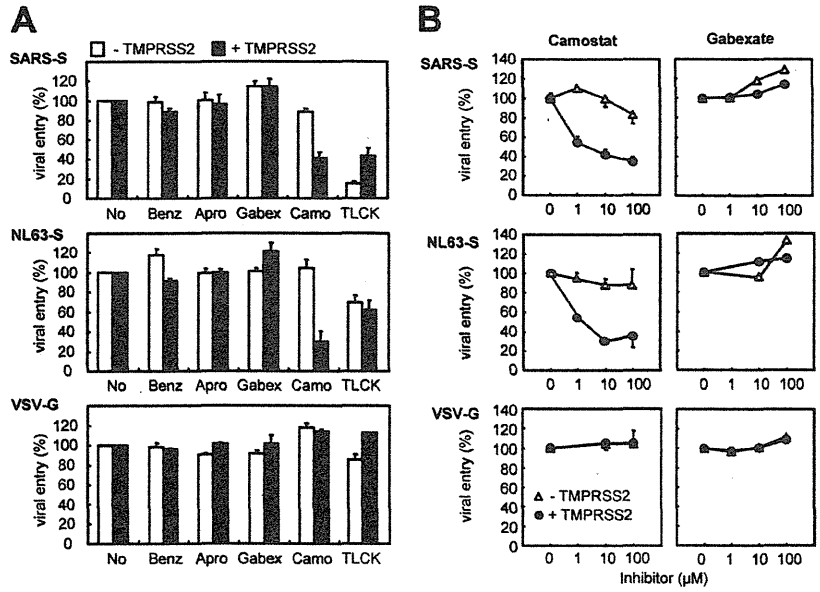

FIG 3 Effects of serine protease inhibitors on viral entry and syncytium formation. (A) HeLa-ACE2 (white bars) and HeLa-ACE2-TMPRSS2 (black bars) cells were infected with pseudotype viruses bearing SARS-S, NL63-S, or VSV-G in the presence of 10 μM benzamidine (Benz), 10 μM aprotinin (Apro), 10 μM gabexate (Gabex), 10 μM camostat (Camo), or 50 μM TLCK. (B) Concentration-dependent effects of inhibitors in HeLa-ACE2 (triangles) or HeLa-ACE2-TMPRSS2 (circles) cells infected with pseudotyped viruses bearing SARS-S, NL63-S, or VSV-G in the presence of serially diluted camostat or gabexate. Infectivity was quantified by counting GFP-positive cells 20 h after viral inoculation. The results are presented as a percentage of infection (at least 200 GFP-positive cells were counted for untreated [No] cells), and error bars indicate the SD of the means from four independent wells.

the acidification of endosomes and thereby also cathepsins, and cytochalasin D, which prevents actin polymerization and therefore endosomal trafficking, were also tested. Figure 5A shows that infection of TMPRSS2-negative cells (white bars) by pseudotyped SARS-S was inhibited about 80% by LIII, but infection by pseudotyped NL63 was only inhibited by 15%. These rates of inhibition are similar to those reported previously (16). Interestingly, inhibition of NL63-S cell entry by bafilomycin A1, EST, and MDL was similar to that of SARS-S cell entry by the same compounds; these results are different from previously reported results (16). Therefore, we carefully tested the concentration-dependent effects of EST and LIII to confirm this difference. Suppression of NL63-S entry was about 80% in the presence of 10 μM to 100 μM EST, but no significant suppression by LIII was observed (Fig. 5B). These results indicate that NL63 utilizes a cysteine protease other than cathepsin L for cell entry.

On the other hand, infection of TMPRSS2-expressing cells (black bars) with pseudotyped SARS-S was inhibited by 30 to 40% in the presence of cathepsin inhibitors and bafilomycin A1, whereas this was not observed for NL63-S infection, except in the

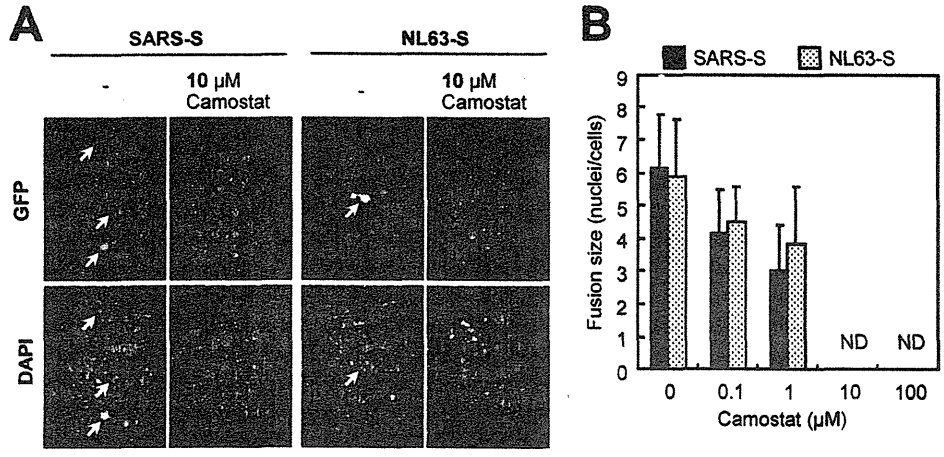

FIG 4 Inhibition of syncytium formation by camostat. (A) Plasmids encoding SARS-S or NL63-S were transfected with plasmid encoding enhanced green fluorescent protein (EGFP) in HeLa-ACE2-TMPRSS2 cells, and incubated in the presence or absence of 10 μM camostat. After 20 h, the cells were fixed with 4% formalin and stained with DAPI. (B) The sizes of syncytia in the absence or presence of 0.1, 1, 10, or 100 μM camostat were quantified by counting the number of nuclei in the fused cells. Error bars indicate the SD of the means from 10 independent syncytia. ND, not determined.

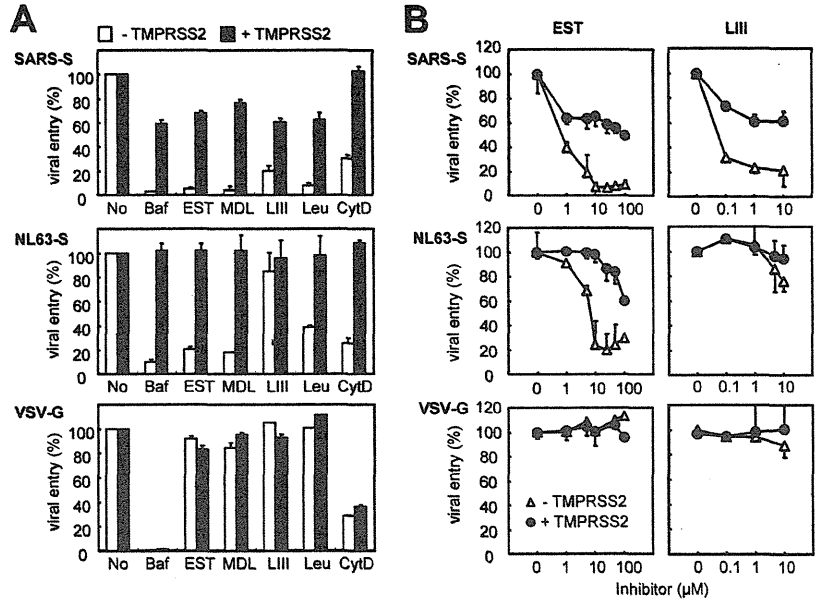

FIG 5 Effects of cathepsin inhibitors or endosome-tropic inhibitors on viral entry. HeLa-ACE2 (white bars) and HeLa-ACE2-TMPRSS2 (black bars) cells were infected with pseudotyped viruses bearing SARS-S, NL63-S, or VSV-G in the presence of 100 nM bafilomycin A1 (Baf), 10 μM EST, 50 μM MDL28170 (MDL), 5 μM cathepsin L inhibitor III (LIII), 50 μM leupeptin (Leu), or 1 μM cytochalasin D (CytD). Infectivity was quantified by counting GFP-positive cells 20 h after viral inoculation. The results are presented as a percentage of infection (at least 200 GFP-positive cells were counted for untreated [No] cells), and error bars indicate the SD of the means from four independent wells.

case of cathepsin L inhibitor III, which inhibited infection by about 15%. These results indicate that 60 to 70% of SARS-S viruses utilize TMPRSS2 rather than cathepsins, whereas 100% of NL63-S viruses utilize TMPRSS2 rather than cathepsins. Furthermore, pseudotyped viruses bearing SARS-S and NL63-S were not inhibited by cytochalasin D in TMPRSS2-expressing cells, although viral inhibition was reduced by >70% in TMPRSS2-negative cells. These results indicated that, in the presence of TMPRSS2, pseudotyped viruses bearing SARS-S and NL63-S complete their entry between the cell surface and early endosome stages.

Inhibition of viral entry by simultaneous treatment with serine and cysteine protease inhibitors. The above results showed that inhibitors of serine and cysteine proteases partially blocked the infection of pseudotyped viruses bearing SARS-S and NL63-S into TMPRSS2-expressing cells. It was therefore of interest to evaluate the effects of simultaneous treatment with both inhibitors on viral entry. TMPRSS2-expressing cells were incubated in medium containing 10 μM EST, 10 μM camostat, or both for 30 min and then infected with the pseudotyped viruses in the presence of inhibitors. Figure 6 shows that simultaneous treatment with camostat and EST dramatically blocked infection, with a decrease of >95%. Similar results were obtained using bafilomycin A1 instead of EST.

Next, we examined the entry speed of these pseudotyped viruses when treated with both EST and camostat. HeLa-ACE2 and HeLa-ACE2-TMPRSS2 were treated with the inhibitors to stop viral entry at the indicated time points after viral adsorption. Cell entry by pseudotyped SARS-S and NL63-S occurred 1 h earlier in cells expressing TMPRSS2 than in nonexpressing cells (Fig. 7). The entry speed of NL63 was slightly higher than that of SARS, as evidenced by the steeper curve for NL63 versus SARS.

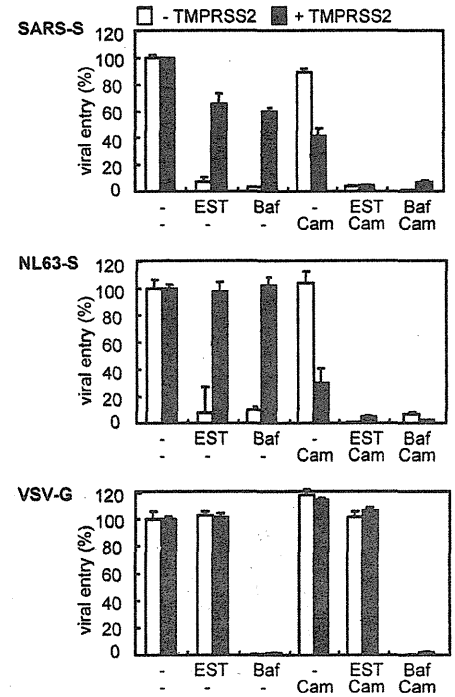

FIG 6 Inhibition of viral entry by simultaneous treatment with serine and cysteine protease inhibitors. HeLa-ACE2 (white bars) and HeLa-ACE2-TMPRSS2 (black bars) cells were infected with pseudotyped viruses bearing SARS-S, NL63-S, or VSV-G in the presence of 10 μM EST, 10 μM camostat (Cam), 100 nM bafilomycin (Baf), both EST and Cam, or both bafilomycin and camostat. Infectivity was quantified by counting GFP-positive cells 20 h after viral inoculation. The results are presented as a percentage of infection (at least 200 GFP-positive cells were counted for untreated cells), and error bars indicate the SD of the means from four independent wells.

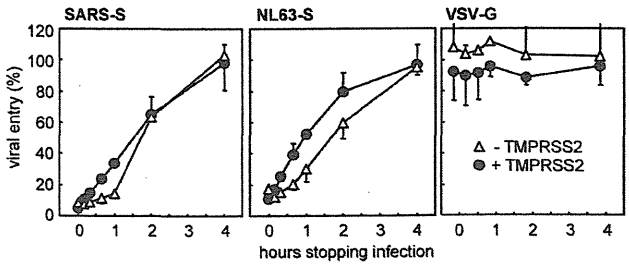

FIG 7 Cell entry kinetics of pseudotyped viruses. Pseudotyped viruses bearing SARS-S, NL63-S, or VSV-G were inoculated onto HeLa-ACE2 (triangles) and HeLa-ACE2-TMPRSS2 (circles) cells and treated with both 10 μM EST and 10 μM camostat to stop viral entry at the indicated time points. Infectivity was quantified by counting GFP-positive cells 20 h after viral inoculation. The results are presented as a percentage of infection (at least 500 GFP-positive cells were counted for untreated cells), and error bars indicate the SD of the means from four independent wells.

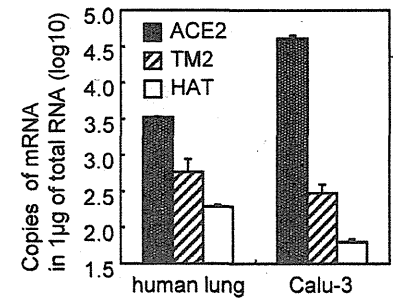

FIG 8 Comparison of transcripts in human lung and Calu-3 cells. The amounts of ACE2, TMPRSS2 (TM2), and HAT mRNA in human lungs or Calu-3 cells were measured using real-time PCR as described in Materials and Methods. Error bars indicate the SD of the means from six independent samples.

Cell entry and multistep growth of authentic SARS-CoV in Calu-3 cells. The above results were obtained in artificially constructed cells expressing TMPRSS2. Thus, the following experiments were performed in Calu-3 cells, an immortalized human airway epithelial cell line regularly used in the study of respiratory pathologies. Unfortunately, Calu-3 cells are not susceptible to VSV pseudotypes because the innate immunity of the cells is thought to suppress the early stages of viral infection. Similarly, Calu-3 is not susceptible to certain other human coronaviruses, such as OC43 and 229E (34), nor were we able to quantitatively determine the level of viral mRNA at 5 h after infection with authentic NL63 (data not shown). Interestingly, authentic SARS-CoV has been reported to infect Calu-3 cells because the SARS-CoV-encoded nsp1 protein suppresses the interferon regulatory factors (34). Therefore, authentic SARS-CoV and real-time PCR were used to detect viral entry and multistep viral growth.

First, ACE2, HAT, and TMPRSS2 mRNA levels were compared in Calu-3 cells and human lung cells. Figure 8 shows that ACE2 mRNA levels were significantly higher and those of TMPRSS2 mRNA were slightly lower in Calu-3 cells than in human lung cells, whereas HAT mRNA was barely detectable in the latter. To test whether SARS-CoV utilizes TMPRSS2 or HAT in Calu-3 cells, the siRNA technique was used to knock down these mRNAs. Calu-3 cells were transiently transfected with siRNAs, and the suppression of the target mRNAs was analyzed by real-time PCR (Fig. 9A). A nontargeting siRNA served as the negative control. However, nontargeting siRNA nonspecifically reduced ACE2, TMPRSS2, and HAT mRNA levels (Fig. 9A), thereby reducing SARS-CoV entry by 10-fold (Fig. 9B). Transfection with a TMPRSS2-specific siRNA resulted in a 10-fold specific decrease of TMPRSS2 mRNA and no effect on ACE2 mRNA in Calu-3 cells compared with nontargeting control transfections. The decrease in HAT mRNA obtained with a HAT-specific siRNA was not evaluated because the amount of remaining transcript was too low to be detectable (Fig. 9A).

Furthermore, SARS-CoV entry into Calu-3 cells was measured in cells treated with siRNA for 4 days followed by additional treatment with EST for 30 min. These cells were then inoculated with SARS-CoV at multiplicities of infection (MOI) of 10 (infectious units were estimated in Vero-E6 cells), and 5 h later, total cellular RNA was isolated. Viral entry was estimated based on newly synthesized viral mRNA9, which was measured quantitatively using real-time PCR. SARS-CoV entry into Calu-3 cells was 1,000-fold lower than that into Vero-E6 cells (data not shown), but was enough to be quantified by real-time PCR. Fig. 9C shows that TMPRSS2-specific siRNA caused efficient inhibition of SARS-CoV cell entry (5-fold decrease), whereas 10 μM EST caused no inhibition. Simultaneous treatment with siRNA and 10 μM EST blocked infection by 10-fold (Fig. 9C). Treatment of the cells with HAT-specific siRNA had no effect on SARS-CoV entry (Fig. 9C).

The effect on Calu-3 cells of simultaneous treatment with SARS-CoV entry inhibitors (i.e., camostat and EST) was also measured. Cells were treated with the inhibitors at 37°C for 30 min, inoculated with SARS-CoV at an MOI of 10, and incubated for 5 h in the presence of the inhibitors. Nontoxic concentrations of inhibitors were used for the experiments in Fig. 10A and C; this was confirmed by measuring mRNA levels of ACE2 and GAPDH by real-time PCR (Fig. 10B and D). Figure 10A shows that 10 μM camostat caused efficient inhibition of viral entry, with a 10-fold decrease, whereas no significant inhibition of SARS-CoV cell entry was obtained with 10 μM EST. However, simultaneous treatment with camostat and EST dramatically blocked infection, with a decrease of 100-fold.

Finally, inhibition of the multistep growth of SARS-CoV was tested in Calu-3 cells. SARS-CoV (10^4 PFU) was inoculated onto 10^6 Calu-3 cells (MOI, 0.01) at 37°C for 2 h. The cells were washed twice with PBS and then incubated for 6 days in the presence or absence of inhibitors. Figure 10C shows that viral replication was suppressed >6,000-fold in cells cultured in the presence of both 10 μM camostat and 10 μM EST. When provided alone, camostat caused a 13-fold decrease in SARS-CoV replication, while EST alone caused a 33-fold decrease. These results indicated that simultaneous treatment with serine and cysteine protease inhibitors efficiently blocked SARS-CoV infection in a human airway epithelial cell line.

DISCUSSION

The interaction of SARS-CoV with host proteases is receptor mediated since the protease cleavage site of S protein is thought to be exposed only after receptor binding (17, 19, 30). During the initial stage of infection, viral utilization of the TMPRSS2 allows for tight temporal control over fusion by protecting the activating cleavage site from premature proteolysis while still allowing efficient cleavage once the virus has bound to target cell receptors. Interestingly, Shulla et al. reported that TMPRSS2 is closely linked to the viral

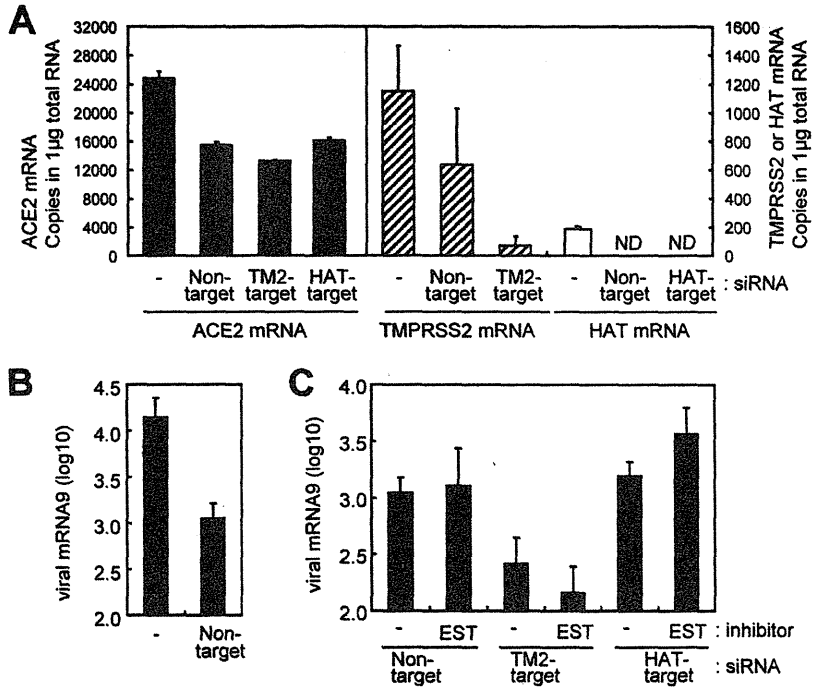

FIG 9 Effect of TMPRSS2 and HAT siRNA-mediated knockdown on SARS-CoV entry into Calu-3 cells. (A) The cells were transiently transfected with siRNAs targeting TMPRSS2 (TM2-target) or HAT (HAT-target) or a nontargeting control ("Non-target"). Nontransfected cells served as the negative control (−). Four days after transfection, cellular RNA was isolated, and ACE2, TMPRSS2, and HAT mRNAs were measured by real-time PCR. (B) Calu-3 cells were infected with SARS-CoV 4 days after transfection of a nontargeting siRNA or nontransfected control (−). Cellular RNA was isolated 5 h after infection, and infectivity was quantified by real-time PCR. (C) Four days after the above-described transfection with siRNA, Calu-3 cells were infected with SARS-CoV in the presence or absence of 10 μM EST. Cellular RNA was isolated 5 h after infection, and infectivity was quantified by real-time PCR measurement of the amount of viral mRNA9. Error bars indicate the SD of the means from six independent samples.

receptor on the target cell surface (27). In the present study, the protease sensitivity of NL63 differed from that of SARS-CoV (Fig. 1). Pseudotyped viruses bearing NL63-S were inactivated by pretreatment with trypsin before cell adsorption, whereas after adsorption, activation occurred only in the presence of a specific concentration of the protease. In contrast, a high concentration of trypsin (1 mg/ml) activated SARS-S infection, indicating that the SARS-CoV S protein is resistant to trypsin (Fig. 1A and B). However, these results using SARS-S were contrary to the findings previously reported by Simmons et al., which showed that trypsin treatment reduced viral infectivity (28, 29). This may be because they added soybean trypsin inhibitor (STI) to stop proteolysis before virus inoculation, whereas we did not. Therefore, in our experiments, trypsin was still active after virus inoculation, indicating that SARS-S is resistant to very high concentrations of trypsin and it retains the ability of infection. Thus, during severe inflammation, NL63 may be inactivated by "free proteases," such as elastase, whereas SARS-CoV is activated. This would explain, at least in part, the different pathogenicities of these two viruses.

Our results indicate that the membrane-anchored protease TMPRSS2 enhances cell entry of both SARS-CoV and HCoV-NL63. NL63 appears to particularly favor TMPRSS2 rather than cathepsin, since in TMPRSS2-expressing cells, pseudotyped NL63-S entry was not inhibited by cathepsin inhibitors at concentrations sufficient to inhibit the infection of TMPRSS2-negative cells (Fig. 5A, middle panel, black versus white bars), although 30 to 40% of SARS-CoV was inhibited by the same inhibitors (Fig. 5A, top panel, black bars). Of note, the present finding of efficient inhibition of cell entry by pseudotyped NL63-S into EST-treated cells without TMPRSS2 (Fig. 5B, middle panel, white triangle) is contrary to previously reported data by Huang et al., (16). Also in contrast to previous results is our observation that bafilomycin A1 inhibited NL63-S entry, whereas ammonium chloride, which also blocks the acidification of endosomes and thereby also cathepsins, was reported not to cause inhibition (16). One possible reason for this difference is cell type: Huang et al. used HEK293 cells, whereas we used HeLa cells. Another reason may be related to use of exogenous trypsin; we often observed an unexpectedly high rate of infection in cells passaged using trypsin (data not shown). Therefore, we used a nonenzymatic cell dissociation solution rather than trypsin.

In the present study, we could not show the cleavage of SARS or NL63-S protein by TMPRSS2 because the cleavage products would be difficult to detect by Western blot analysis. We previously reported that a considerable amount of cleavage of SARS-CoV S protein was not detected, and Shulla et al. reported that only very low levels of S cleavage were detected in cells expressing TMPRSS2 (19, 27). Also, we previously reported that the S protein of mouse hepatitis virus type 2 (MHV-2), which is very similar to the S protein of SARS-CoV, is cleaved by trypsin only after conformational changes induced by receptor binding (21). Therefore, we hypothesized that only a small amount of S protein needs to be cleaved to enable viral or cell-cell membrane fusion by TMPRSS2.

Previous studies showed that SARS-CoV is able to enter cells

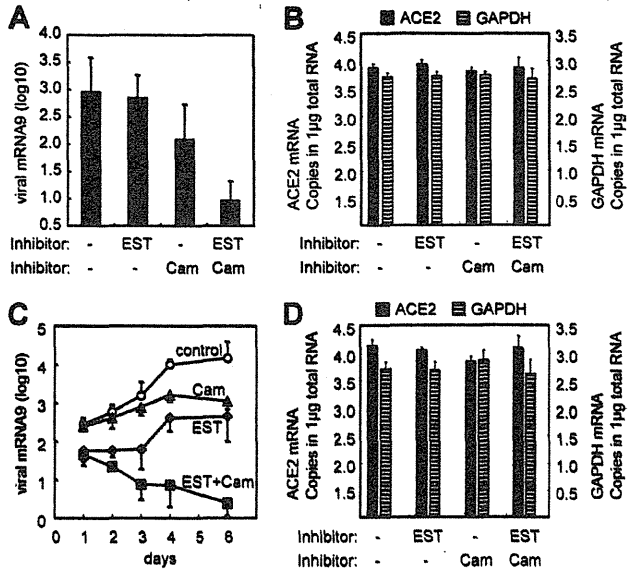

FIG 10 Inhibition of viral entry and multistep growth of SARS-CoV in Calu-3 cells after simultaneous treatment with inhibitors. (A) Calu-3 cells were infected with SARS-CoV at an MOI of 10 in the presence of 10 μM camostat (Cam), 10 μM EST, or both. Five hours later, cellular RNA was isolated and infectivity was quantified by real-time PCR. (B) The mRNA levels for a housekeeping gene (GAPDH) and for the virus receptor (ACE2) were measured to evaluate the nontoxicity of camostat and EST in the same Calu-3 cells for which the infectivity results are shown in panel A. (C) Calu-3 cells were infected with SARS-CoV at an MOI of 0.01 for 1 h at 37°C, and then the cells were incubated in the presence of 10 μM camostat, 10 μM EST, or both. Nontreated cells served as the negative control. Cellular RNA was isolated on the indicated days. (D) GAPDH and ACE2 mRNA levels were measured to evaluate the nontoxicity of camostat and EST in the samples at 6 days postinfection (shown in panel C). Infectivity was quantified by real-time PCR measurement of the amount of viral mRNA9. Error bars indicate the SD of the means from six independent samples.

via two distinct pathways, depending on the specific proteases present on the cell surface (19, 20, 30). As seen in Fig. 6, simultaneous treatment with EST and camostat significantly inhibited the entry of pseudotyped viruses into TMPRSS2-expressing HeLa cells, which suggests that both pathways must be blocked to prevent cell entry of SARS-CoV and HCoV-NL63. Also, the multistep growth of SARS-CoV in Calu-3 cells was significantly inhibited by simultaneous treatment with both inhibitors at 4 days and at 6 days, while separate treatment with camostat and EST caused only a partial decrease in SARS-CoV infection. This also indicates that both pathways need to be blocked to prevent SARS-CoV infection in lung-derived cells. On the other hand, we found that SARS-CoV enters Calu-3 cells through the cell surface (TMPRSS2) route rather than through the endosomal (cathepsins) route during initial viral entry, since siRNA targeting of TMPRSS2 caused a 5-fold decrease and camostat treatment caused a 10-fold decrease in SARS-CoV entry into Calu-3 cells, whereas viral entry was not blocked by EST (Fig. 9C and 10A). Therefore, it was unclear whether endosomal cathepsins or cell surface proteases are mainly utilized during viral entry.

Knowledge of which route (the cell surface, the endosome, or both) is mainly utilized by coronavirus in the human lungs will enable the choice of a suitable inhibitor, which could then be used as a candidate antiviral drug. It is important to note that SARS-CoV is highly pathogenic only in the lungs, although the receptor is expressed on the vesicular endothelial cells of all organs. This implies that lung-specific rather than ubiquitous enzymes determine viral tropism and pathogenesis. For example, SARS-CoV might utilize a lung-specific protease such as TMPRSS2 rather than cathepsins. This in turn suggests that camostat is a suitable candidate as an antiviral drug to prevent SARS-CoV infection in the lungs. Camostat is already being prescribed for the suppression of pancreatitis-induced pain due to its ability to inhibit pancreatic and other inflammatory proteases, including elastase (31). Therefore, camostat can inhibit *in vivo* infection by SARS-CoV and other pneumoviruses, such as influenza A and metapneumovirus virus, as all of these viruses are known to utilize TMPRSS2. Naturally, this strategy must first be confirmed in animal models.

ACKNOWLEDGMENTS

We thank Makoto Ujike (NVLU.ac.jp), Kazuhiko Kanou (NIH.go.jp), Masako Abe (NIH.go.jp), Koji Sakai (NIH.go.jp), and Makoto Takeda (NIH.go.jp) for valuable suggestions.

This work was financially supported by grants from the Ministry of Education, Culture, Sports, Science and Technology (Japan), the Ministry of Health, Labor and Welfare (Japan), the Mochida Memorial Foundation, and Telumo Life Science Foundation.

REFERENCES

1. Belouzard S, Chu VC, Whittaker GR. 2009. Activation of the SARS coronavirus spike protein via sequential proteolytic cleavage at two distinct sites. Proc. Natl. Acad. Sci. U. S. A. 106:5871–5876.
2. Belouzard S, Madu I, Whittaker GR. 2010. Elastase-mediated activation of the severe acute respiratory syndrome coronavirus spike protein at discrete sites within the S2 domain. J. Biol. Chem. 285:22758–22763.
3. Bertram S, et al. 2010. TMPRSS2 and TMPRSS4 facilitate trypsin-independent spread of influenza virus in Caco-2 cells. J. Virol. 84:10016–10025.
4. Bertram S, et al. 2011. Cleavage and activation of the severe acute respiratory syndrome coronavirus spike protein by human airway trypsin-like protease. J. Virol. 85:13363–13372.
5. Bertram S, Glowacka I, Steffen I, Kühl A, Pöhlmann S. 2010. Novel insights into proteolytic cleavage of influenza virus hemagglutinin. Rev. Med. Virol. 20:298–310.
6. Bosch BJ, Bartelink W, Rottier PJM. 2008. Cathepsin L functionally cleaves the severe acute respiratory syndrome coronavirus class I fusion protein upstream of rather than adjacent to the fusion peptide. J. Virol. 82:8887–8890.
7. Böttcher E, Freuer C, Steinmetzer T, Klenk H-D, Garten W. 2009. MDCK cells that express proteases TMPRSS2 and HAT provide a cell system to propagate influenza viruses in the absence of trypsin and to study cleavage of HA and its inhibition. Vaccine 27:6324–6329.
8. Böttcher E, et al. 2006. Proteolytic activation of influenza viruses by serine proteases TMPRSS2 and HAT from human airway epithelium. J. Virol. 80:9896–9898.
9. Böttcher-Friebertshäuser E, et al. 2010. Cleavage of influenza virus hemagglutinin by airway proteases TMPRSS2 and HAT differs in subcellular localization and susceptibility to protease inhibitors. J. Virol. 84:5605–5614.
10. Böttcher-Friebertshäuser E, Stein DA, Klenk H-D, Garten W. 2011. Inhibition of influenza virus infection in human airway cell cultures by an antisense peptide-conjugated morpholino oligomer targeting the hemagglutinin-activating protease TMPRSS2. J. Virol. 85:1554–1562.
11. Chaipan C, et al. 2009. Proteolytic activation of the 1918 influenza virus hemagglutinin. J. Virol. 83:3200–3211.
12. Choi S-Y, Bertram S, Glowacka I, Park YW, Pöhlmann S. 2009. Type II transmembrane serine proteases in cancer and viral infections. Trends Mol. Med. 15:303–312.
13. Ding Y, et al. 2003. The clinical pathology of severe acute respiratory syndrome (SARS): a report from China. J. Pathol. 200:282–289.
14. Fukushi S, et al. 2005. Vesicular stomatitis virus pseudotyped with severe acute respiratory syndrome coronavirus spike protein. J. Gen. Virol. 86:2269–2274.

15. **Glowacka I, et al.** 2011. Evidence that TMPRSS2 activates the severe acute respiratory syndrome coronavirus spike protein for membrane fusion and reduces viral control by the humoral immune response. J. Virol. 85:4122–4134.
16. **Huang I-C, et al.** 2006. SARS coronavirus, but not human coronavirus NL63, utilizes cathepsin L to infect ACE2-expressing cells. J. Biol. Chem. 281:3198–3203.
17. **Kam Y-W, et al.** 2009. Cleavage of the SARS coronavirus spike glycoprotein by airway proteases enhances virus entry into human bronchial epithelial cells in vitro. PLoS One 4:e7870. doi:10.1371/journal.pone.0007870.
18. **Kawase M, Shirato K, Matsuyama S, Taguchi F.** 2009. Protease-mediated entry via the endosome of human coronavirus 229E. J. Virol. 83:712–721.
19. **Matsuyama S, et al.** 2010. Efficient activation of the severe acute respiratory syndrome coronavirus spike protein by the transmembrane protease TMPRSS2. J. Virol. 84:12658–12664.
20. **Matsuyama S, Ujike M, Morikawa S, Tashiro M, Taguchi F.** 2005. Protease-mediated enhancement of severe acute respiratory syndrome coronavirus infection. Proc. Natl. Acad. Sci. U. S. A. 102:12543–12547.
21. **Matsuyama S, Taguchi F.** 2009. Two-step conformational changes in a coronavirus envelope glycoprotein mediated by receptor binding and proteolysis. J. Virol. 83:11133–11141.
22. **Miyauchi K, Kim Y, Latinovic O, Morozov V, Melikyan GB.** 2009. HIV enters cells via endocytosis and dynamin-dependent fusion with endosomes. Cell 137:433–444.
23. **Okumura Y, et al.** 2010. Novel type II transmembrane serine proteases, MSPL and TMPRSS13, proteolytically activate membrane fusion activity of the hemagglutinin of highly pathogenic avian influenza viruses and induce their multicycle replication. J. Virol. 84:5089–5096.
24. **Paoloni-Giacobino A, Chen H, Peitsch MC, Rossier C, Antonarakis SE.** 1997. Cloning of the TMPRSS2 gene, which encodes a novel serine protease with transmembrane, LDLRA, and SRCR domains and maps to 21q22.3. Genomics 44:309–320.
25. **Shirato K, Matsuyama S, Ujike M, Taguchi F.** 2011. Role of proteases in the release of porcine epidemic diarrhea virus from infected cells. J. Virol. 85:7872–7880.
26. **Shirogane Y, et al.** 2008. Efficient multiplication of human metapneumovirus in Vero cells expressing the transmembrane serine protease TMPRSS2. J. Virol. 82:8942–8946.
27. **Shulla A, et al.** 2011. A transmembrane serine protease is linked to the severe acute respiratory syndrome coronavirus receptor and activates virus entry. J. Virol. 85:873–882.
28. **Simmons G, et al.** 2011. Different host cell proteases activate the SARS-coronavirus spike-protein for cell-cell and virus-cell fusion. Virology 413: 265–274.
29. **Simmons G, et al.** 2005. Inhibitors of cathepsin L prevent severe acute respiratory syndrome coronavirus entry. Proc. Natl. Acad. Sci. U. S. A. 102:11876–11881.
30. **Simmons G, et al.** 2004. Characterization of severe acute respiratory syndrome-associated coronavirus (SARS-CoV) spike glycoprotein-mediated viral entry. Proc. Natl. Acad. Sci. U. S. A. 101:4240–4245.
31. **Talukdar R, Tandon RK.** 2008. Pancreatic stellate cells: new target in the treatment of chronic pancreatitis. J. Gastroenterol. Hepatol. 23:34–41.
32. **To KF, Lo AWI.** 2004. Exploring the pathogenesis of severe acute respiratory syndrome (SARS): the tissue distribution of the coronavirus (SARS-CoV) and its putative receptor, angiotensin-converting enzyme 2 (ACE2). J. Pathol. 203:740–743.
33. **Watanabe R, et al.** 2008. Entry from the cell surface of severe acute respiratory syndrome coronavirus with cleaved S protein as revealed by pseudotype virus bearing cleaved S protein. J. Virol. 82:11985–11991.
34. **Yoshikawa T, et al.** 2010. Dynamic innate immune responses of human bronchial epithelial cells to severe acute respiratory syndrome-associated coronavirus infection. PLoS One 5:e8729. doi:10.1371/journal.pone.0008729.

Journal of Virology

Efficient Activation of the Severe Acute Respiratory Syndrome Coronavirus Spike Protein by the Transmembrane Protease TMPRSS2

Shutoku Matsuyama, Noriyo Nagata, Kazuya Shirato, Miyuki Kawase, Makoto Takeda and Fumihiro Taguchi

J. Virol. **2010, 84(24):12658. DOI: 10.1128/JVI.01542-10.**
Published Ahead of Print 6 October 2010.

JOURNAL OF VIROLOGY, Dec. 2010, p. 12658–12664 Vol. 84, No. 24
0022-538X/10/$12.00 doi:10.1128/JVI.01542-10

Efficient Activation of the Severe Acute Respiratory Syndrome Coronavirus Spike Protein by the Transmembrane Protease TMPRSS2[▽]

Shutoku Matsuyama,[1]* Noriyo Nagata,[2] Kazuya Shirato,[1] Miyuki Kawase,[1] Makoto Takeda,[1] and Fumihiro Taguchi[3]

Departments of Virology III[1] and Pathology,[2] National Institute of Infectious Diseases, Japan, 4-7-1 Gakuen Musashi-Murayama, Tokyo 208-0011, Japan, and Faculty of Veterinary Medicine, Nippon Veterinary and Life Science University, 1-7-1 Sakai-minami Musasino, Tokyo 180-8602, Japan[3]

Received 23 July 2010/Accepted 28 September 2010

The distribution of the severe acute respiratory syndrome coronavirus (SARS-CoV) receptor, an angiotensin-converting enzyme 2 (ACE2), does not strictly correlate with SARS-CoV cell tropism in lungs; therefore, other cellular factors have been predicted to be required for activation of virus infection. In the present study, we identified transmembrane protease serine 2 (TMPRSS2), whose expression does correlate with SARS-CoV infection in the upper lobe of the lung. In Vero cells expressing TMPRSS2, large syncytia were induced by SARS-CoV infection. Further, the lysosome-tropic reagents failed to inhibit, whereas the heptad repeat peptide efficiently inhibited viral entry into cells, suggesting that TMPRSS2 affects the S protein at the cell surface and induces virus-plasma membrane fusion. On the other hand, production of virus in TMPRSS2-expressing cells did not result in S-protein cleavage or increased infectivity of the resulting virus. Thus, TMPRSS2 affects the entry of virus but not other phases of virus replication. We hypothesized that the spatial orientation of TMPRSS2 vis-a-vis S protein is a key mechanism underling this phenomenon. To test this, the TMPRSS2 and S proteins were expressed in cells labeled with fluorescent probes of different colors, and the cell-cell fusion between these cells was tested. Results indicate that TMPRSS2 needs to be expressed in the opposing (target) cell membrane to activate S protein rather than in the producer cell, as found for influenza A virus and metapneumoviruses. This is the first report of TMPRSS2 being required in the target cell for activation of a viral fusion protein but not for the S protein synthesized in and transported to the surface of cells. Our findings suggest that the TMPRSS2 expressed in lung tissues may be a determinant of viral tropism and pathogenicity at the initial site of SARS-CoV infection.

Angiotensin-converting enzyme 2 (ACE2) has been shown to be the functional receptor for severe acute respiratory syndrome coronavirus (SARS-CoV) (18, 24), the etiological agent of an acute infectious disease that spreads mainly via the respiratory route. Although ACE2 is present in the vascular endothelial cells of all organs, SARS-CoV is highly pathogenic only in the lungs (12). Furthermore, while ACE2 expression in the lung has been shown for both type I and type II pneumocytes (12), cell tropism of SARS-CoV does not strictly correlate with ACE2 expression, suggesting that other factors are required to explain the pathogenesis of this disease (8, 32). One such factor is the critical role played by host cellular proteases in the process of viral entry into cells. For example, a variety of proteases such as trypsin, tryptase Clara, miniplasmin, human airway trypsin-like protease (HAT), and TMPRSS2 (transmembrane protease, serine 2) are known to cleave the glycoprotein hemagglutinin (HA) of influenza A viruses, a prerequisite for the fusion between viral and host cell membranes and viral cell entry. Cleavage of HA is critical for viral infection, with the tissue distribution of proteases determining cell tropism of virus strains (16). There are two major mechanisms responsible for proteolytic activation of viral glycoproteins. For many viruses, such as the human immunodeficiency virus (HIV) and Nipah virus, cellular proteases (e.g., furin or cathepsin) cleave the glycoprotein during biogenesis, separating receptor binding and fusion subunits and converting the precursor glycoprotein to its fusion-competent state (36). Alternatively, for other viruses such as Ebola and SARS-CoV, cleavage of the viral glycoprotein by endosomal proteases induces conformational changes during viral entry following receptor binding and/or endocytosis (6, 20, 28, 31).

Three proteases—trypsin, cathepsin L, and elastase—have been previously reported to activate the spike (S) protein of SARS-CoV (3, 13, 20, 30, 31). In the absence of proteases at the cell surface, SARS-CoV enters cells by an endosomal pathway, and S protein is activated for fusion by cathepsin L in the endosome (14, 30, 37). Conversely, in the presence of proteases at the cell surface, such as trypsin and elastase, viral S proteins attached to the receptor at the host cell surface are activated, inducing envelope-plasma membrane fusion and direct entry of SARS-CoV into cells (21). Viral replication in the latter case has been shown to be 100 times higher than replication via the endosomal pathway (21), suggesting that the higher infectivity of SARS-CoV in the lungs could be due to an enhancement of direct viral cell entry mediated by proteases. In this study we test the possibility that TMPRSS2 is an acti-

* Corresponding author. Mailing address: Department of Virology III, National Institute of Infectious Diseases, Japan, 4-7-1 Gakuen, Musashi-Murayama, Tokyo 208-0011, Japan. Phone: 81 42 561 0771, ext. 3755. Fax: 81 42 567 5631. E-mail: matuyama@nih.go.jp.

[▽] Published ahead of print on 6 October 2010.

vator of SARS-CoV entry into host cells. TMPRSS2 is highly expressed at epithelial cells in human lungs (9, 26) and activates influenza A virus and metapneumovirus in culture cells (4, 5, 7, 29). Here, we present data indicating that the distribution of TMPRSS2 correlates with SARS-CoV infection in the lung and that this protease can efficiently activate SARS-CoV S protein to induce virus-cell membrane fusion at the cell surface.

MATERIALS AND METHODS

Animal experiments. Animal experiments with SARS-CoV-infected cynomolgus monkeys were performed as described previously (23). Briefly, 3-year-old male cynomolgus monkeys were intratracheally inoculated with 108 50% tissue culture infective doses ($TCID_{50}$) of SARS-CoV. On day 7 postinoculation animals were euthanized, and tissue samples of the lungs were collected.

Immunofluorescence staining method. Detection of TMPRSS2, ACE2, and SARS-CoV antigens was performed on paraffin-embedded sections by a double immunofluorescence staining method modified from a previous protocol (19, 22, 23). Rabbit antibody (Ab) against TMPRSS2 (ab56110; Abcam), goat antibody against recombinant human ACE2 (R&D Systems, MN), and the SKOT9 monocional mouse antibody against nucleocapsid protein of SARS-CoV (25) were used as primary antibodies. Briefly, after deparaffinization with xylene, the sections were rehydrated in ethanol and immersed in phosphate-buffered saline (PBS). Antigens were retrieved by hydrolytic autoclaving in the retrieval solution at pH 9.0 (Nichirei). After a cooling step, normal donkey or goat serum was used to block background staining. To detect the TMPRSS2 or ACE2 antigen, the sections were immersed in PBS and then incubated with primary antibodies overnight at 4°C. After three washes in PBS, the sections were incubated with monoclonal antibody for 60 min at 37°C to detect the SARS-CoV protein. After three additional washes in PBS, the sections were incubated with anti-rabbit (goat origin) or anti-goat (donkey origin) Alexa Fluor 546 and anti-mouse (goat or donkey origin) Alexa Fluor 488 (Molecular Probes, Eugene, OR) for 60 min at 37°C to detect the primary antibodies,. The sections were mounted with ProLong antifade reagent with 4',6'-diamidino-2-phenylindole (DAPI; Molecular Probes), and images were captured and analyzed by confocal laser microscopy (Fluoview FV1000-D; Olympus, Tokyo, Japan).

Cells and viruses. Vero E6 and Vero cells and Vero cells expressing TMPRSS2 (Vero-TMPRSS2) (29) were cultured in Dulbecco's modified Eagle's medium (DMEM; Gibco/BRL), supplemented with 5% fetal bovine serum (Gibco/BRL). The SARS-CoV Frankfurt 1 strain, kindly provided by J. Ziebuhr (University of Würzburg, Germany), and the recombinant vaccinia virus containing the gene encoding the spike protein of SARS-CoV (Dis/SARS-S), kindly provided by K. Ishii (NIID, Japan), were propagated and assayed by using Vero E6 and 293T cells, respectively.

Virus entry assay. Vero or Vero-TMPRSS2 cells in 96-well plates were treated with DMEM containing the reagents indicated in the legends of Fig. 3 at 37°C for 30 min and then chilled on ice for 10 min. Approximately 105 PFU (PFU) of virus in DMEM was used to infect 106 cells on ice. After an adsorption period of 30 min, the virus was removed, and infected cells were cultured in DMEM with the reagents at 37°C for 5 h. Viral mRNAs were isolated from cells with the addition of 200 μl of Isogen (Nippon gene). Real-time PCR was performed to estimate the amounts of newly synthesized mRNA9 as described previously (21).

Western blotting. Expression of S protein in Vero E6 cells was analyzed by Western blotting. Preparation of cell lysates, SDS-PAGE, and electrical transfer of the protein onto a transfer membrane were described elsewhere (21). S protein was detected with anti-S antibody (IMG-557; Imgenex, San Diego) and anti-rabbit IgG-horseradish peroxidase (HRPO). Influenza virus HA was detected with anti-HA Ab, Udorn virus HA (29), and anti-goat IgG-HRPO. Bands were visualized by using enhanced chemiluminescence reagents (ECL Plus; Amersham Pharmacia) on an LAS-1000 instrument (Fuji).

Cell-cell fusion. Effector cells (Vero or Vero-TMPRSS2) were infected with Dis/SARS-S at a multiplicity of infection (MOI) of 1 for 1 h or transfected with pKS/SARS-S by using the Fugene 6 reagent (Roche) and then labeled with 2 μM CellTracker Green (5-chloromethylfluorescein diacetate [CMFDA] Invitrogen) for 30 min and washed three times with medium. Meanwhile, Vero or Vero-TMPRSS2 target cells were labeled with 2 μM orange chloromethyl tetramethylrhodamine (CMTMR; Invitrogen) for 30 min and washed three times with medium. Effector cells were collected with nonenzymatic cell dissociation solution (Sigma) and then overlaid on target cells. Cells were incubated for 20 h and observed by fluorescence microscopy (BioZero, Keyence) for cell-cell fusion. The extent of syncytium formation was semiquantified by counting the number of nuclei in the S-protein-expressing cells (10 syncytia).

RESULTS

Distribution of TMPRSS2 in the SARS-CoV-infected cynomolgus lung. We examined the immunohistochemical distribution of TMPRSS2 and ACE2 in the uninfected lung of cynomolgus monkeys. TMPRSS2 antigens were detected in type I pneumocytes (Fig. 1A, arrows indicating thin shapes in middle panel), whereas only weak staining of ACE2 antigens was detected in enlarged type II pneumocytes (Fig. 1C, arrows indicating round shapes in middle panel) by the immunofluorescence staining method used. An antibody against SARS-CoV was used as a negative control (Fig. 1A and C, upper left panels). In addition, the histopathology of SARS-CoV-infected lungs was examined on day 7 postinoculation as described previously (23). Mild lesions with some regenerated type II epithelial cells were observed in the upper lobe (Fig. 1B and D,). SARS-CoV antigens were detected in the cytoplasm of type I pneumocytes (Fig. 1B and D, arrowheads), which primarily resembled TMPRSS2-expressing cells (Fig. 1B, upper right) more than ACE2-expressing cells (Fig. 1D, upper right). In contrast, severe pulmonary edema and inflammatory reactions were observed in severe lesions (Fig. 1B and D). Marked immunostaining of TMPRSS2 and ACE2 antigens was detected in the cytoplasm of enlarged type II pneumocytes (Fig. 1B and D, lower middle panels). SARS-CoV antigens were detected in the cytoplasm of many unspecified cells (Fig. 1B and D, lower left), but these cells never merged with either TMPRSS2- or ACE2-expressing cells. These results suggest that the presence of SARS-CoV antigens does not correlate with the presence of either ACE2 or TMPRSS2 antigens in severe lesions.

Syncytium formation by SARS-CoV infection of TMPRSS2-expressing cells. Vero cells have been generally used for infection assays of SARS-CoV (10). SARS-CoV S protein-expressing Vero cells form syncytia if treated with trypsin but not in its absence (Fig. 2B, frames a and c). Here, we examined whether Vero cells stably expressing TMPRSS2 (VERO-TMPRSS2) undergo syncytium formation induced by SARS-CoV infection or S-protein expression. After 36 h of SARS-CoV infection at an MOI of 0.1, large syncytia were observed in Vero-TMPRSS2 cells (Fig. 2A, frame b) but not in Vero cells (Fig. 2A, frame a). To determine if expression of S protein induced syncytium formation, Vero-TMPRSS2 cells were infected with vaccinia virus encoding the SARS-CoV S gene, Dis/SARS-S, which resulted in the formation of large syncytia at 20 h after infection (Fig. 2B, frame b). In addition, plasmid-based expression of S protein also induced syncytia (see Fig. 5B). To further assess if TMPRSS2 can proteolytically activate S protein, Vero-TMPRSS2 cells expressing S protein were treated with various concentrations of leupeptin (Fig. 2C), a known inhibitor of serine and cysteine proteases. The results show that syncytium formation was moderately inhibited at a concentration of 500 μM (Fig. 2C, frame b, and D) and completely inhibited at a concentration of 5 mM (Fig. 2C, frame c, and D), suggesting that leupeptin inhibits the activity of TMPRSS2, suppressing S-protein-induced cell-cell fusion.

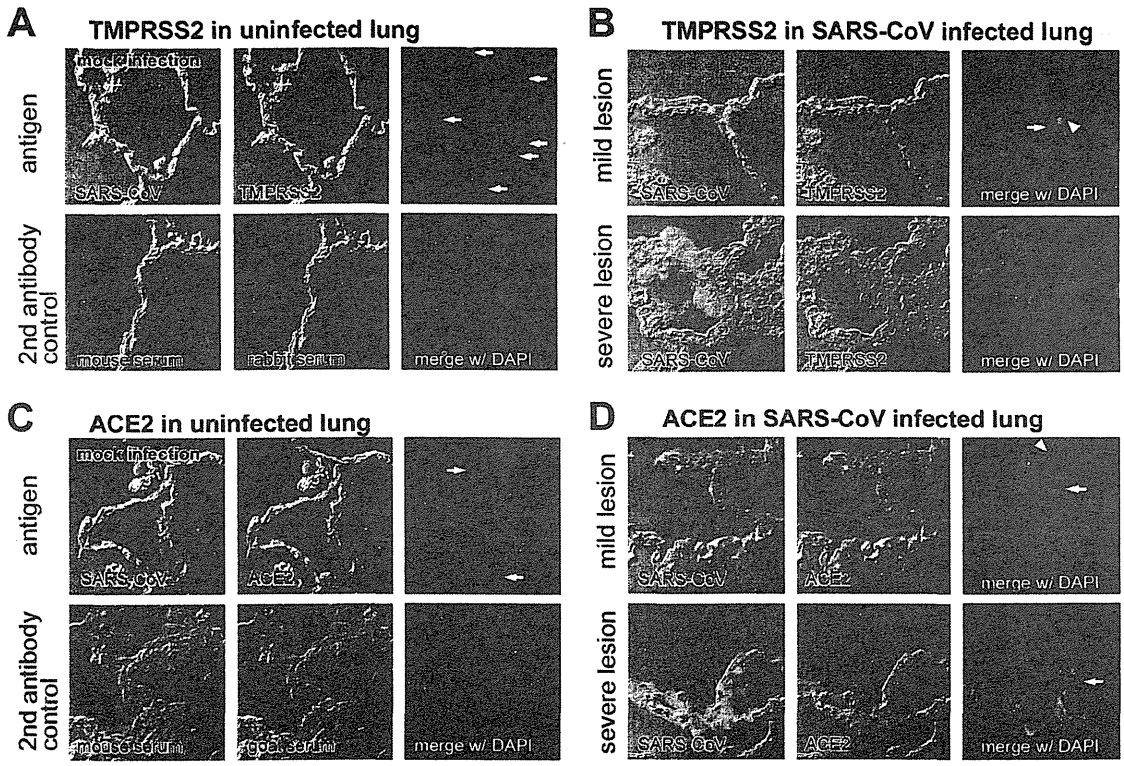

FIG. 1. Distribution of TMPRSS2 and ACE2 and histopathology of SARS-CoV-infected cynomolgus lung. The distribution of TMPRSS2 (A, arrows indicating round shapes in middle panel) and ACE2 (C, arrows indicating thin shapes in middle panel) in healthy cynomolgus lung sections stained with antibodies against SARS-CoV, TMPRSS2, or DAPI (upper panels) was detected by an immunofluorescence staining method (see Materials and Methods section). Samples stained with secondary antibodies were used as controls (lower panels). The distribution of TMPRSS2 (B) and ACE2 (D) was also examined in mild (upper row) and severe (lower row) lesions of SARS-CoV-infected lungs stained with antibodies against SARS-CoV, TMPRSS2, or DAPI (nuclear staining).

Viral entry into TMPRSS2-expressing cells. The above observations suggest that TMPRSS2 activates S protein at the cell surface, enabling viral entry into the cell. To assess this possibility, we first examined the effects of EST (Calbiochem), which is known to inhibit endosomal cathepsins and thereby block infection of Vero cells by SARS-CoV (35). Viral entry into cells was estimated by the newly synthesized viral mRNA9, which was quantified by real-time PCR as described previously (21). As shown in Fig. 3, treatment of Vero cells with EST at a concentration of 50 μM caused a 1,000-fold decrease of SARS-CoV cell entry via the endosomal pathway. In contrast, EST failed to suppress viral entry into Vero-TMPRSS2 cells. Similarly, treatment with bafilomycin A (Sigma) at a concentration of 500 μM reduced infectivity by 100-fold in Vero cells although only mild suppression (10%) of viral infection was observed in Vero-TMPRSS2 cells. Furthermore, we examined the effect of heptad repeat 2 (HR2) peptide, kindly provided by R. S. Hodges (33), on SARS-CoV infectivity in Vero-TMPRSS2 cells. HR2 peptide is known to prevent trypsin-activated cell entry of SARS-CoV via the cell surface; presumably an S protein activated by cell surface receptor exposes the HR1 region, and the HR2 peptide then interferes with the six-helix bundle formation (34). Treatment with HR2 peptide at a concentration of 5 μM efficiently suppressed viral entry into Vero-TMPRSS2 cells but not into Vero cells. These results suggest that TMPRSS2 activates S protein and facilitates viral entry via the cell surface.

TMPRSS2 does not cleave SARS-CoV S during virus production. It has been previously shown that TMPRSS2 expressed in cells promoted cleavage of glycoprotein of influenza A virus and metapneumovirus, increasing infectivity (5, 29). Here, we examined whether the S protein of SARS-CoV is cleaved and activated in Vero-TMPRSS2 cells. After 36 h of infection of Vero and Vero-TMPRSS2 cells with SARS-CoV, cells and medium were collected, and Western blotting was performed to detect S protein. As shown in Fig. 4A (right), the HA of influenza virus was markedly cleaved in Vero-TMPRSS2 cells at 18 h after transfection. However, S proteins synthesized in either Vero or Vero-TMPRSS2 cells were not cleaved when examined in cell lysates or in virions released into the medium (Fig. 4A, left). Furthermore, the infectious titers of SARS-CoV produced in Vero and Vero-TMPRSS2 (on Vero E6 cells) were not markedly different, and in both cases infection was inhibited by bafilomycin A1 but not HR2 peptide (Fig. 4B). These results suggest that SARS-CoV produced in Vero-TMPRSS2 cells has no fusion-competent, cleaved S protein entering into cells via the endosomal pathway.

Productive activation of S by TMPRSS2 requires TMPRSS2 expression in target cells. The previous results suggest that

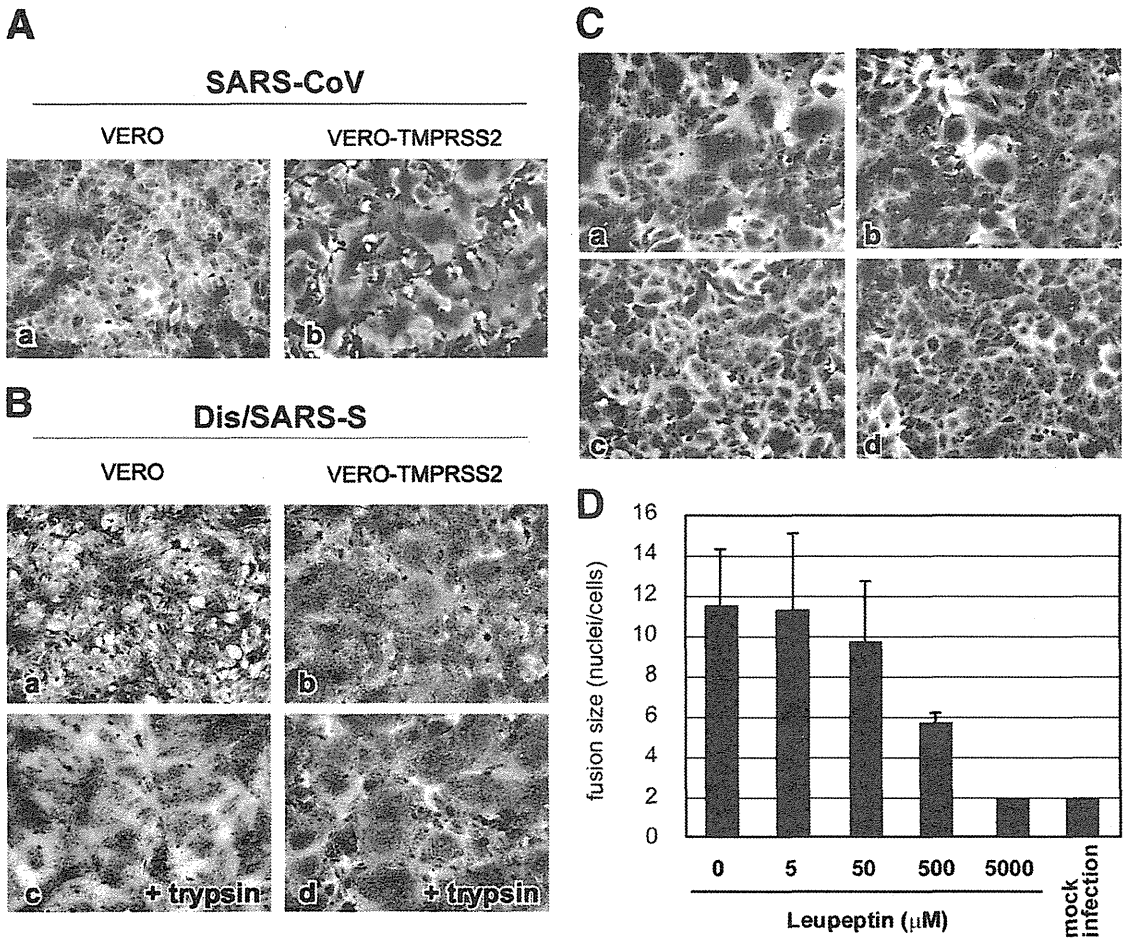

FIG. 2. Cytopathic changes on SARS-CoV S-protein-expressing cells. (A) Vero cells or Vero-TMPRSS2 cells were infected with SARS-CoV at an MOI of 0.1 and incubated at 37°C for 36 h. Cells were stained with crystal violet. (B) Vero cells or Vero-TMPRSS2 cells were infected with Dis/SARS-S at an MOI of 0.1 and incubated at 37°C for 20 h, after which the cells were treated with 10 μg/ml trypsin at 37°C for 30 min and then incubated for another 3 h. (C) Vero-TMPRSS2 cells were infected with Dis/SARS-S at an MOI of 0.1 and incubated at 37°C for 20 h in the absence (a) or presence of 500 μM (b) or 5 mM (c) leupeptin. Cells not infected with Dis/SARS-S were used as a control (d). (D) The size of syncytia in the absence and presence of 5 μM, 50 μM, 500 μM, and 5 mM leupeptin was quantified by counting the number of nuclei in the fused cells. The error bars are standard deviations.

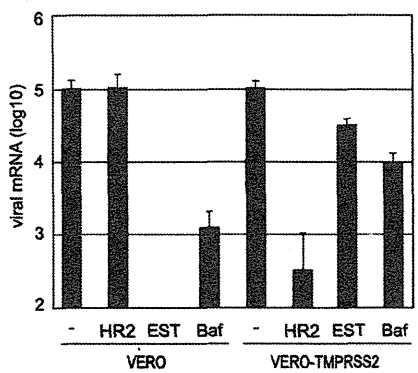

FIG. 3. Effect of TMPRSS2 on virus entry into cells. Vero or Vero-TMPRSS2 cells were infected with SARS-CoV at an MOI of 0.1 in the presence of 5 μM HR2 peptide, 50 μM EST, or 500 μM bafilomycin A1 and then cultured for 5 h. The amount of viral mRNA9 was measured by real-time PCR. Cells not treated with reagents were used as controls. The error bars are standard deviations of at least six independent measurements.

TMPRSS2 affects viral S protein attached to receptors at the cell surface but not newly synthesized S proteins either during transport to the plasma membrane or incorporation into the virion. We hypothesized that the spatial orientation of TMPRSS2 against S protein might be critical for S protein activation. To demonstrate this spatial dependence between TMPRSS2 and S protein, a cell-cell fusion assay was conducted. Our design is diagramed in Fig. 5A. Vero and Vero-TMPRSS2 cells were either Dis/SARS-S infected (Fig. 5B, frames a, b, c, and d) or pKS/SARS-S transfected (Fig. 5B, frames e, f, g, and h) to express S protein and then stained with green as described in the methodology. The green-labeled Vero and Vero-TMPRSS2 cells were collected with nonenzymatic cell dissociation solution and overlaid onto the orange-labeled target cells, Vero and Vero-TMPRSS2. As shown in Fig. 5B, the formation of syncytia was not induced in cells not expressing TMPRSS2 (Fig. 5B, frames a and e). Also, syncytia were not formed between green cells expressing

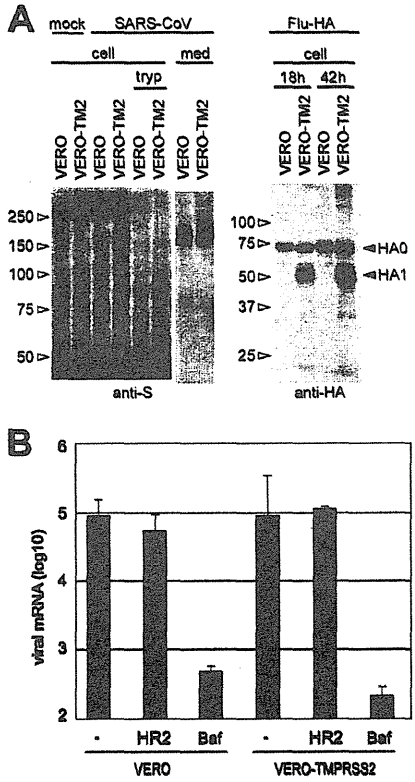

FIG. 4. TMPRSS2 does not affect virus production. (A) SDS-PAGE and Western blot analysis were performed to detect S protein in cell lysates (cell) and culture medium (med) of Vero or Vero-TMPRSS2 (Vero-TM2) cells at 20 h after SARS-CoV infection (left panel). Cells treated with 10 μg/ml trypsin (tryp) at 37°C for 5 min were used as a cleaved-S control. Influenza virus (Flu)-HA produced by plasmid transfection was also used as a cleavage control (right panel). (B) Infectivity of SARS-CoV produced in Vero or Vero-TMPRSS2 cells. Vero-E6 cells were infected with SARS-CoV produced in either Vero or Vero-TMPRSS2 cells in the presence of 5 μM HR2 peptide or 500 nM bafilomycin A1 and then cultured for 5 h. The amount of viral mRNA9 was measured by real-time PCR. Cells not treated with reagents were used as controls. The error bars are standard deviations of at least six independent measurements.

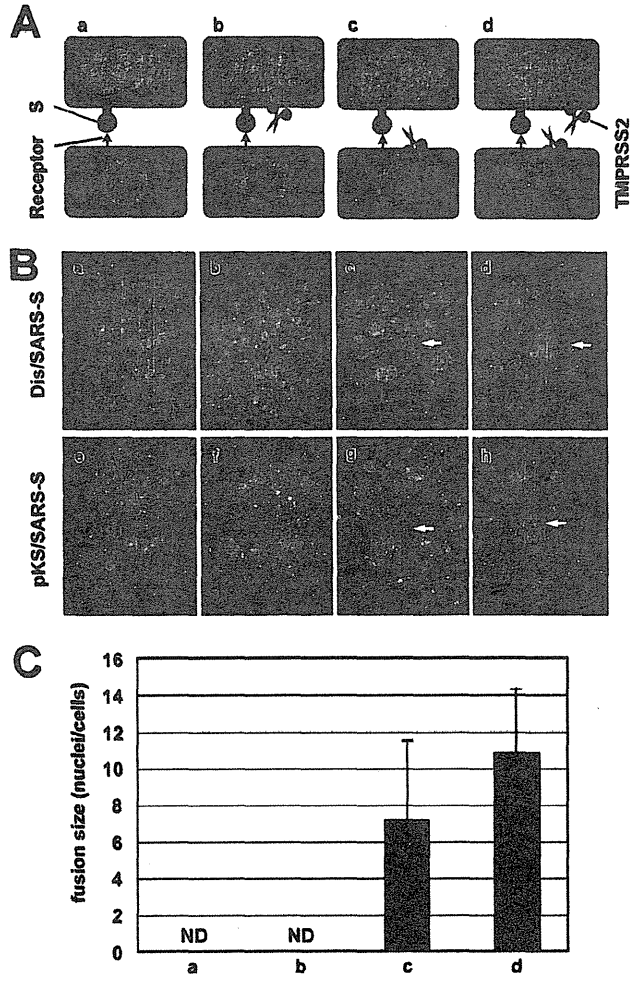

FIG. 5. TMPRSS2 dependence on spatial orientation for the activation of SARS-CoV S protein. (A) Schematic diagrams of S-expressing effector cells (green) and acceptor cells (orange) shown in panel B. (B) To detect cell-cell fusion of S-expressing cells, Dis/SARS-S-infected or pKS/SARS-S-transfected Vero or Vero-TMPRSS2 cells (effector cells) were collected by nonenzymatic cell dissociation solution and then overlaid onto the orange target Vero or Vero-TMPRSS2 cells, respectively. After 20 h of incubation, cells were fixed with 4% formaldehyde and observed by fluorescence microscopy. White arrows indicate fused cells. (C) The sizes of syncytia indicated in the upper row of panel B were quantified by counting the number of nuclei in the fused cells. The error bars are standard deviations.

both TMPRSS2 and S protein and the orange Vero cells without TMPRSS2 (Fig. 5B, frames b and f). However, large syncytia were formed when TMPRSS2 was expressed either in the orange target cells (Fig. 5B, frames c and g) or both in the orange target and green producer cells (Fig. 5B, frames d and h). The extent of syncytium formation was semiquantified by counting the number of nuclei in the fused cells infected with Dis/SARS-S (Fig. 5C). It was previously reported that ACE2 is downregulated in S-expressing cells (11, 17), indicating that green producer cells are refractory to self-fusion due to a lack of receptors at the cell surface. These results suggest that the spatial orientation of TMPRSS2 must be opposite that of S protein (namely, the two proteins must reside in opposite membranes) to induce membrane fusion. This observation is in agreement with the idea that TMPRSS2 activates only viral S protein already attached to receptors at the cell surface but not during virus maturation.

DISCUSSION

In the present study we showed the distribution of ACE2 in mild and severe inflammatory lesions of cynomolgus lungs infected by SARS-CoV. We found that type II pneumocytes, which are frequently observed in regenerated tissues during inflammation and which express high levels of ACE2, were refractory to SARS-CoV infection, whereas type I pneumocytes, which do not express detectable levels of ACE2, were readily infected by SARS-CoV. This inconsistency may be explained by the downregulation of ACE2 in SARS-CoV-infected cells, as previously reported (11, 17). Here, we showed that the localization of TMPRSS2-expressing cells in normal lung tissues, rather than ACE2-expressing cells, is closely tied

to SARS-CoV infection in mild lesions, indicating that TMPRSS2 may determine viral tropism at an early stage of SARS-CoV infection. However, TMPRSS2 expression occurred in cells adjacent to virus-infected cells, not in infected cells, suggesting that TMPRSS2 may also be downregulated in infected cells, as observed for ACE2. We have previously reported that SARS-CoV infectivity was enhanced in culture cells by the addition of exogenous elastase, which enabled virus entry via the cell surface (21). Elastase is a major protease produced by neutrophils during inflammation and may be relevant to the high level of SARS-CoV replication in lungs that results in severe pneumonia in the mouse model (1). We have also reported that in the late stage of SARS-CoV infection in the cynomolgus lung, which remarkably occurs with severe inflammation in the lower lobe, SARS-CoV is distributed in both type I and type II pneumocytes (23), indicating that elastase may trigger viral entry via the surface of these cells and determine SARS-CoV pathogenicity in this late stage of infection.

Activation of viral glycoprotein by TMPRSS2 has been previously reported for influenza A virus and metapneumovirus (4, 5, 7, 29). The most distinctive difference between these viruses and SARS-CoV is the stage during virus replication in which viral glycoproteins are cleaved by proteases. In influenza A virus and metapneumovirus, the protease makes a simple cut in the glycoprotein during maturation, in a manner similar to that made by furin. In contrast, SARS-CoV S protein is cleaved by the protease following receptor-induced conformational changes. The protease cleavage site in S protein, located nearer the C-terminal region than predicted for a cleavage site, is thought to be exposed only after receptor binding (2, 35). In support of this model, we recently reported that the S protein of mouse hepatitis virus type 2 (MHV-2), which is highly similar to the S protein of SARS-CoV (27), requires two-step conformational changes mediated by sequential receptor binding and proteolysis to be activated for fusion (20). Such a mechanism allows for tight temporal control over fusion by protecting the activating cleavage site from premature proteolysis yet allowing efficient cleavage upon binding to the receptor on target cells.

Previous studies have clearly demonstrated that the SARS-CoV S protein requires proteolytic cleavage for S-mediated cell-cell or virus-cell fusion (3, 13, 21, 30, 31). Recently, the cleavage of S protein by the airway transmembrane protease, TMPRSS11a, was also reported (15). Treatment with a purified soluble form of TMPRSS11a following receptor binding to the pseudotyped SARS-CoV S protein strongly enhanced viral infection. Moreover, proteolytic cleavage by TMPRSS11a was observed at the same position as cleavage by trypsin in the purified soluble form of S protein (15). While the reported concentration of the previously mentioned proteases required to induce membrane fusion is extremely high (3, 15, 21), the amount of TMPRSS2 expressed in Vero-TMPRSS2 cells is thought to be low (29). Still, our results showed the formation of massive syncytia when S protein was expressed (Fig. 2), suggesting that TMPRSS2 may be more efficient than previously characterized proteases. The inhibition of cell-cell fusion in TMPRSS2-expressing cells in the presence of a protease inhibitor (Fig. 2) strongly suggests that TMPRSS2 proteolytically affects S protein. Because we could not detect a considerable amount of cleaved S protein in cells expressing both S and TMPRSS2, even when massive syncytia were observed in these cells, we hypothesized that proteolytic activation of S protein by TMPRSS2 occurs only during cell entry, following receptor binding. The results shown in Fig. 5 support this hypothesis and clearly show that the spatial orientation of TMPRSS2 in relation to S protein is a key mechanism underling this phenomenon: TMPRSS2 must be expressed in the opposing cell membrane to activate S protein and induce cell-cell fusion. We speculate that the encounter of receptor-bound S protein with TMPRSS2 at the right time and in the correct spatial orientation at the cell surface results in efficient cleavage of S protein and subsequent membrane fusion. Therefore, only a small amount of S protein needs to be cleaved to enable viral or cell-cell membrane fusion. These cleavage products would be difficult to detect by Western blot analysis.

Additionally, we have previously reported that HR2 peptide inhibits SARS-CoV entry into Vero E6 cells in the presence, but not the absence, of trypsin. Likewise, inhibition of SARS-CoV cell entry does not occur when the virus is allowed to use the normal endosomal, cathepsin L-dependent, entry pathway (34). Here, we show (Fig. 3) that HR2 peptide efficiently inhibits viral entry into TMPRSS2-expressing cells. This result provides further evidence that TMPRSS2 is efficient for viral entry and is localized at the cell surface, exposing the HR2 peptide binding site before endocytosis can occur. Thus, even if HR2 peptide does not efficiently work in commonly used tissue cell cultures, it may be a suitable candidate antiviral for the inhibition of SARS-CoV infection of lung cells that express membrane-associated proteases.

ACKNOWLEDGMENTS

We thank S. E. Delos and J. M. White (University of Virginia) for valuable comments on this work. We also thank R. S. Hodges (University of Colorado, Denver, CO) and K. Ishii (National Institute of Infectious Diseases, Japan) for providing us with HR2 peptide and Dis/SARS-S, respectively.

This work was supported by an MEXT grant and by grants from the Uehara Memorial Foundation and the Ichiro Kanehara Foundation.

REFERENCES

1. **Ami, Y., N. Nagata, K. Shirato, R. Watanabe, N. Iwata, K. Nakagaki, S. Fukushi, M. Saijo, S. Morikawa, and F. Taguchi.** 2008. Co-infection of respiratory bacterium with severe acute respiratory syndrome coronavirus induces an exacerbated pneumonia in mice. Microbiol. Immunol. **52:**118–127.
2. **Belouzard, S., V. C. Chu, and G. R. Whittaker.** 2009. Activation of the SARS coronavirus spike protein via sequential proteolytic cleavage at two distinct sites. Proc. Natl. Acad. Sci. U. S. A. **106:**5871–5876.
3. **Bosch, B. J., W. Bartelink, and P. J. M. Rottier.** 2008. Cathepsin L functionally cleaves the severe acute respiratory syndrome coronavirus class I fusion protein upstream of rather than adjacent to the fusion peptide. J. Virol. **82:**8887–8890.
4. **Böttcher, E., T. Matrosovich, M. Beyerle, H. Klenk, W. Garten, and M. Matrosovich.** 2006. Proteolytic activation of influenza viruses by serine proteases TMPRSS2 and HAT from human airway epithelium. J. Virol. **80:** 9896–9898.
5. **Chaipan, C., D. Kobasa, S. Bertram, I. Glowacka, I. Steffen, T. S. Tsegaye, M. Takeda, T. H. Bugge, S. Kim, Y. Park, A. Marzi, and S. Pöhlmann.** 2009. Proteolytic activation of the 1918 influenza virus hemagglutinin. J. Virol. **83:**3200–3211.
6. **Chandran, K., N. J. Sullivan, U. Felbor, S. P. Whelan, and J. M. Cunningham.** 2005. Endosomal proteolysis of the Ebola virus glycoprotein is necessary for infection. Science **308:**1643–1645.
7. **Choi, S., S. Bertram, I. Glowacka, Y. W. Park, and S. Pöhlmann.** 2009. Type II transmembrane serine proteases in cancer and viral infections. Trends Mol. Med. **15:**303–312.
8. **Ding, Y., H. Wang, H. Shen, Z. Li, J. Geng, H. Han, J. Cai, X. Li, W. Kang,**

D. Weng, Y. Lu, D. Wu, L. He, and K. Yao. 2003. The clinical pathology of severe acute respiratory syndrome (SARS): a report from China. J. Pathol. **200**:282–289.
9. **Donaldson, S. H., A. Hirsh, D. C. Li, G. Holloway, J. Chao, R. C. Boucher, and S. E. Gabriel.** 2002. Regulation of the epithelial sodium channel by serine proteases in human airways. J. Biol. Chem. **277**:8338–8345.
10. **Drosten, C., S. Günther, W. Preiser, S. van der Werf, H. R. Brodt, S. Becker, H. Rabenau, M. Panning, L. Kolesnikova, R. A. Fouchier, A. Berger, A. M. Burguière, J. Cinatl, M. Eickmann, N. Escriou, K. Grywna, S. Kramme, J. C. Manuguerra, S. Müller, V. Rickerts, M. Stürmer, S. Vieth, H. D. Klenk, A. D. Osterhaus, H. Schmitz, and H. W. Doerr.** 2003. Identification of a novel coronavirus in patients with severe acute respiratory syndrome. N. Engl. J. Med. **348**:1967–1976.
11. **Glowacka, I., S. Bertram, P. Herzog, S. Pfefferle, I. Steffen, M. O. Muench, G. Simmons, H. Hofmann, T. Kuri, F. Weber, J. Eichler, C. Drosten, and S. Pöhlmann.** 2010. Differential downregulation of ACE2 by the spike proteins of SARS-coronavirus and human coronavirus NL63. J. Virol. **84**:1198–1205.
12. **Hamming, I., W. Timens, M. L. C. Bulthuis, A. T. Lely, G. J. Navis, and H. van Goor.** 2004. Tissue distribution of ACE2 protein, the functional receptor for SARS coronavirus. A first step in understanding SARS pathogenesis. J. Pathol. **203**:631–637.
13. **Huang, I., B. J. Bosch, F. Li, W. Li, K. H. Lee, S. Ghiran, N. Vasilieva, T. S. Dermody, S. C. Harrison, P. R. Dormitzer, M. Farzan, P. J. M. Rottier, and H. Choe.** 2006. SARS coronavirus, but not human coronavirus NL63, utilizes cathepsin L to infect ACE2-expressing cells. J. Biol. Chem. **281**:3198–3203.
14. **Inoue, Y., N. Tanaka, Y. Tanaka, S. Inoue, K. Morita, Z. Min, T. Hattori, and K. Sugamura.** 2007. Clathrin-dependent entry of severe acute respiratory syndrome coronavirus into target cells expressing ACE2 with the cytoplasmic tail deleted. J. Virol. **81**:8722–8729.
15. **Kam, Y., Y. Okumura, H. Kido, L. F. P. Ng, R. Bruzzone, and R. Altmeyer.** 2009. Cleavage of the SARS coronavirus spike glycoprotein by airway proteases enhances virus entry into human bronchial epithelial cells in vitro. PloS One **4**:e7870.
16. **Kido, H., Y. Okumura, E. Takahashi, H. Pan, S. Wang, J. Chida, T. Q. Le, and M. Yano.** 2008. Host envelope glycoprotein processing proteases are indispensable for entry into human cells by seasonal and highly pathogenic avian influenza viruses. J. Mol. Gen. Med. **3**:167–175.
17. **Kuba, K., Y. Imai, S. Rao, H. Gao, F. Guo, B. Guan, Y. Huan, P. Yang, Y. Zhang, W. Deng, L. Bao, B. Zhang, G. Liu, Z. Wang, M. Chappell, Y. Liu, D. Zheng, A. Leibbrandt, T. Wada, A. Slutsky, D. Liu, C. Qin, C. Jiang, and J. Penninger.** 2005. A crucial role of angiotensin converting enzyme 2 (ACE2) in SARS coronavirus-induced lung injury. Nat. Med. **11**:875–879.
18. **Li, W., M. Moore, N. Vasilieva, J. Sui, S. K. Wong, M. Berne, M. Somasundaran, J. Sullivan, K. Luzuriaga, T. Greenough, H. Choe, and M. Farzan.** 2003. Angiotensin-converting enzyme 2 is a functional receptor for the SARS coronavirus. Nature **426**:450–454.
19. **Liem, N. T., N. Nakajima, L. P. Phat, Y. Sato, H. N. Thach, P. V. Hung, L. T. San, H. Katano, T. Kumasaka, T. Oka, S. Kawachi, T. Matsushita, T. Sata, K. Kudo, and K. Suzuki.** 2008. H5N1-infected cells in lung with diffuse alveolar damage in exudative phase from a fatal case in Vietnam. Jpn. J. Infect. Dis. **61**:157–160.
20. **Matsuyama, S., and F. Taguchi.** 2009. Two-step conformational changes in a coronavirus envelope glycoprotein mediated by receptor binding and proteolysis. J. Virol. **83**:11133–11141.
21. **Matsuyama, S., M. Ujike, S. Morikawa, M. Tashiro, and F. Taguchi.** 2005. Protease-mediated enhancement of severe acute respiratory syndrome coronavirus infection. Proc. Natl. Acad. Sci. U. S. A. **102**:12543–12547.
22. **Nagata, N., N. Iwata, H. Hasegawa, S. Fukushi, A. Harashima, Y. Sato, M. Saijo, F. Taguchi, S. Morikawa, and T. Sata.** 2008. Mouse-passaged severe acute respiratory syndrome-associated coronavirus leads to lethal pulmonary edema and diffuse alveolar damage in adult but not young mice. Am. J. Pathol. **172**:1625–1637.
23. **Nagata, N., N. Iwata, H. Hasegawa, Y. Sato, S. Morikawa, M. Saijo, S. Itamura, T. Saito, Y. Ami, T. Odagiri, M. Tashiro, and T. Sata.** 2007. Pathology and virus dispersion in cynomolgus monkeys experimentally infected with severe acute respiratory syndrome coronavirus via different inoculation routes. Int. J. Exp. Pathol. **88**:403–414.
24. **Nie, Y., P. Wang, X. Shi, G. Wang, J. Chen, A. Zheng, W. Wang, Z. Wang, X. Qu, M. Luo, L. Tan, X. Song, X. Yin, J. Chen, M. Ding, and H. Deng.** 2004. Highly infectious SARS-CoV pseudotyped virus reveals the cell tropism and its correlation with receptor expression. Biochem. Biophys. Res. Commun. **321**:994–1000.
25. **Ohnishi, K., M. Sakaguchi, T. Kaji, K. Akagawa, T. Taniyama, M. Kasai, Y. Tsunetsugu-Yokota, M. Oshima, K. Yamamoto, N. Takasuka, S. Hashimoto, M. Ato, H. Fujii, Y. Takahashi, S. Morikawa, K. Ishii, T. Sata, H. Takagi, S. Itamura, T. Odagiri, T. Miyamura, I. Kurane, M. Tashiro, T. Kurata, H. Yoshikura, and T. Takemori.** 2005. Immunological detection of severe acute respiratory syndrome coronavirus by monoclonal antibodies. Jpn. J. Infect. Dis. **58**:88–94.
26. **Paoloni-Giacobino, A., H. Chen, M. C. Peitsch, C. Rossier, and S. E. Antonarakis.** 1997. Cloning of the TMPRSS2 gene, which encodes a novel serine protease with transmembrane, LDLRA, and SRCR domains and maps to 21q22.3. Genomics **44**:309–320.
27. **Qiu, Z., S. T. Hingley, G. Simmons, C. Yu, J. Das Sarma, P. Bates, and S. R. Weiss.** 2006. Endosomal proteolysis by cathepsins is necessary for murine coronavirus mouse hepatitis virus type 2 spike-mediated entry. J. Virol. **80**:5768–5776.
28. **Schornberg, K., S. Matsuyama, K. Kabsch, S. Delos, A. Bouton, and J. White.** 2006. Role of endosomal cathepsins in entry mediated by the Ebola virus glycoprotein. J. Virol. **80**:4174–4178.
29. **Shirogane, Y., M. Takeda, M. Iwasaki, N. Ishiguro, H. Takeuchi, Y. Nakatsu, M. Tahara, H. Kikuta, and Y. Yanagi.** 2008. Efficient multiplication of human metapneumovirus in Vero cells expressing the transmembrane serine protease TMPRSS2. J. Virol. **82**:8942–8946.
30. **Simmons, G., D. N. Gosalia, A. J. Rennekamp, J. D. Reeves, S. L. Diamond, and P. Bates.** 2005. Inhibitors of cathepsin L prevent severe acute respiratory syndrome coronavirus entry. Proc. Natl. Acad. Sci. U. S. A. **102**:11876–11881.
31. **Simmons, G., J. D. Reeves, A. J. Rennekamp, S. M. Amberg, A. J. Piefer, and P. Bates.** 2004. Characterization of severe acute respiratory syndrome-associated coronavirus (SARS-CoV) spike glycoprotein-mediated viral entry. Proc. Natl. Acad. Sci. U. S. A. **101**:4240–4245.
32. **To, K. F., and A. W. I. Lo.** 2004. Exploring the pathogenesis of severe acute respiratory syndrome (SARS): the tissue distribution of the coronavirus (SARS-CoV) and its putative receptor, angiotensin-converting enzyme 2 (ACE2). J. Pathol. **203**:740–743.
33. **Tripet, B., D. J. Kao, S. A. Jeffers, K. V. Holmes, and R. S. Hodges.** 2006. Template-based coiled-coil antigens elicit neutralizing antibodies to the SARS-coronavirus. J. Struct. Biol. **155**:176–194.
34. **Ujike, M., H. Nishikawa, A. Otaka, N. Yamamoto, N. Yamamoto, M. Matsuoka, E. Kodama, N. Fujii, and F. Taguchi.** 2008. Heptad repeat-derived peptides block protease-mediated direct entry from the cell surface of severe acute respiratory syndrome coronavirus but not entry via the endosomal pathway. J. Virol. **82**:588–592.
35. **Watanabe, R., S. Matsuyama, K. Shirato, M. Maejima, S. Fukushi, S. Morikawa, and F. Taguchi.** 2008. Entry from the cell surface of severe acute respiratory syndrome coronavirus with cleaved S protein as revealed by pseudotype virus bearing cleaved S protein. J. Virol. **82**:11985–11991.
36. **White, J., S. Delos, M. Brecher, and K. Schornberg.** 2008. Structures and mechanisms of viral membrane fusion proteins: multiple variations on a common theme. Crit. Rev. Biochem. Mol. Biol. **43**:189–219.
37. **Yang, Z., Y. Huang, L. Ganesh, K. Leung, W. Kong, O. Schwartz, K. Subbarao, and G. J. Nabel.** 2004. pH-dependent entry of severe acute respiratory syndrome coronavirus is mediated by the spike glycoprotein and enhanced by dendritic cell transfer through DC-SIGN. J. Virol. **78**:5642–5650.

Leukemia (2010) 24, 914–923

www.nature.com/leu

ORIGINAL ARTICLE

Elevated PIN1 expression by C/EBPα-p30 blocks C/EBPα-induced granulocytic differentiation through c-Jun in AML

JA Pulikkan[1], V Dengler[1], AA Peer Zada[1], A Kawasaki[2,3], M Geletu[1], Z Pasalic[4,5], SK Bohlander[4,5], A Ryo[6], DG Tenen[2,3] and G Behre[1]

[1]State Center for Cell and Gene Therapy, Department of Oncology and Hematology, Martin Luther University Halle-Wittenberg, Halle, Germany; [2]Harvard Stem Cell Institute, Harvard Medical School, Boston, USA; [3]Cancer Science Institute, National University of Singapore, Singapore; [4]Department of Medicine III, University of Munich, Munich, Germany; [5]Clinical Cooperative Group, HelmholtzZentrum 'German Research Center for Environmental Health', Munich, Germany and [6]AIDS Research center, National Institute of Infectious Diseases, Tokyo, Japan

The transcription factor CCAAT enhancer-binding protein α (C/EBPα) has an important role in granulopoiesis. The tumor suppressor function of C/EBPα is shown by the findings that loss of expression or function of C/EBPα in leukemic blasts contributes to a block in myeloid cell differentiation and to leukemia. C/EBPα mutations are found in around 9% of acute myeloid leukemia (AML) patients. The mechanism by which the mutant form of C/EBPα (C/EBPα-p30) exerts a differentiation block is not well understood. By using a proteomic screen, we have recently reported PIN1 as a target of C/EBPα-p30 in AML. In the present study, we show that C/EBPα-p30 induces PIN1 expression. We observed elevated PIN1 expression in leukemic patient samples. Induction of C/EBPα-p30 results in recruitment of E2F1 in the PIN1 promoter. We show that the inhibition of PIN1 leads to myeloid differentiation in primary AML blasts with C/EBPα mutations. Overexpression of PIN1 in myeloid cells leads to block of granulocyte differentiation. We also show that PIN1 increases the stability of the c-Jun protein by inhibiting c-Jun ubiquitination, and c-Jun blocks granulocyte differentiation mediated by C/EBPα. Our data suggest that the inhibition of PIN1 could be a potential strategy of treating AML patients with C/EBPα mutation.
Leukemia (2010) **24**, 914–923; doi:10.1038/leu.2010.37; published online 8 April 2010
Keywords: C/EBPα; PIN1; AML

Introduction

The transcription factor CCAAT enhancer-binding protein α (C/EBPα) is a critical regulator of the myeloid differentiation program. Recent studies on animal models and acute myeloid leukemia (AML) patient samples suggest that the loss of function or expression of C/EBPα provides a platform on which AML develops.[1] C/EBPα is mutated in about 9% of AML samples.[2] The mutations reported in C/EBPα are point mutations in the basic region or in the leucine zipper domain and frame shift mutations in the N-terminal domain, which result in the expression of the shorter form of C/EBPα, C/EBPα-p30.[3,4] C/EBPα-p30 is produced by alternative transcription initiation. It retains the DNA-binding domain, but lacks the N-terminal transactivation domain of the longer form of C/EBPα, C/EBPα-p42. C/EBPα-p30 fails to induce differentiation and exhibits a dominant-negative function over C/EBPα-p42. The expression of the p30 isoform is high in AML patients with C/EBPα mutations. A recent study has shown the ability of C/EBPα-p30 to induce AML in a mouse model.[5]

Using a proteomic approach, we have recently shown that one of the mechanisms behind the dominant-negative function of C/EBPα-p30 is through increased sumoylation of C/EBPα-p42 by UBC9.[6] In this screen, we also identified the peptidyl–prolyl *cis/trans* isomerase, PIN1, as one of the transcriptional target genes of C/EBPα-p30. PIN1 binds to and isomerizes the peptidyl–prolyl bond in serine or threonine-phosphorylated Ser/Thr-Pro motifs.[7,8] PIN1 appears to be important in tumorigenesis because it has been found to be overexpressed in many cancers including prostate, lung, ovary, cervical, breast, brain and skin cancers.[9,10]

Although *Pin1*-null animals display age-dependent defects, no other phenotypic characteristics related to cancer have been detected.[11] Mice lacking *Pin1* are resistant to tumorigenesis induced by oncogenic Neu or Ras.[12] The inhibition of PIN1 in cancer cells by multiple approaches triggers apoptosis or suppresses the transformed phenotype.[13,14]

Indirect evidence for the role of PIN1 in leukemia comes from its positive effect on the transcriptional activity of c-Jun,[10,15] a protooncogene shown by our lab to be downregulated by C/EBPα-p42 during granulopoiesis.[16] We have also shown that c-Jun is overexpressed in AML patients with C/EBPα mutations.[17] Furthermore, growing number of studies support the oncogenic potential of PIN1, which is an E2F1 target.[18] Interestingly, E2F1 inhibition by C/EBPα is a critical step in myeloid differentiation.[19] However, the exact role of PIN1 in leukemogenesis remains elusive.

In the present study, we investigated the role of PIN1 in AML with C/EBPα mutation. We provide evidence that C/EBPα-p30 upregulates PIN1 protein levels. AML patients show high PIN1 expression. We show that silencing PIN1 leads to granulocytic differentiation of primary AML blasts derived from patients with C/EBPα mutations and also in leukemic cell lines. Furthermore, we show that PIN1 prevents degradation of c-Jun, which in turn blocks C/EBPα-induced differentiation.

Materials and methods

Cells, transfections and reagents

Kasumi-6 cells were obtained from ATCC (Manassas, VA, USA). Blast cells from AML patients were obtained from the Laboratory for Leukemia Diagnostics at the University of Munich, Germany.

Correspondence: Dr G Behre, Universitätsklinikum Halle (Saale), Klinik für Innere Medizin IV—Onkologie/Hämatologie -Ernst-Grube-Straße 40, 06120 Halle, Germany.
E-mail: gerhard.behre@medizin.uni-halle.de
Received 23 April 2009; revised 9 January 2010; accepted 2 February 2010; published online 8 April 2010

All samples were karyotyped and molecular genetic analysis was performed for C/EBPα mutations. Before therapy, all patients gave their informed consent for participation in the Acute Myeloid Leukemia Cooperative Group (AMLCG) studies. Details of the study protocol have been published.[20]

K562-C/EBPα-p42-ER and K562-C/EBPα-p30-ER cells[21] were maintained in RPMI 1640 medium without phenol red, supplemented with 10% charcoal-treated fetal bovine serum, 1% penicillin-streptomycin and 2 μg/ml puromycin; Kasumi-6 cells[22] were cultured in RPMI 1640 medium supplemented with 20% fetal bovine serum, 1% penicillin-streptomycin and 2 ng/ml granulocyte–macrophage colony-stimulating factor; AML blast cells were cultured in Iscove's modified Dulbecco's medium supplemented with 10% fetal bovine serum, 1% penicillin-streptomycin and 20 mM HEPES (4-(2-hydroxyethyl)-1-piperazineethanesulfonic acid); U937 cells and NB4 cells were cultured in RPMI medium supplemented with 10% fetal bovine serum and 1% penicillin-streptomycin.

K562-C/EBPα-p30-BRM2-ER cells were established as reported before.[21] Briefly, C/EBPα-p30 was amplified by PCR using rat C/EBPα having BRM2 mutation (kind gift from Bruno Calabretta) with *Bam*HI flanking primers (forward primer 5′-GGGGATCCGCCACCATGTCCGCGGGGGCGCAC-3′ and reverse primer 5′-ATGGATCCGGCGCGCAGTTG-3′) and subsequently cloned into pBabe-ER digested with *Bam*HI with the 30-KDa C/EBPα peptide in frame with the C-terminal endoplasmic reticulum (ER) domain. K562 cells (10^6 cells) were electroporated with AMAXA transfection method with 3 μg of *Sca*I-linearized plasmid and plated on six-well plate containing phenol red-free RPMI/10% charcoal-treated fetal bovine serum medium. Selection with 1 μg/ml puromycin began 48 h after transfection.

Cells (2×10^4 293T cells) were transfected with the Lipofectamine Plus reagent (Invitrogen, Karlsruhe, Germany) according to manufacturer's instruction. Transfection of U937 and Kasumi-6 cells was performed with the Nucleofector kit (AMAXA, Cologne, Germany) as described by the manufacturer. Plasmid DNA (2 μg) was used for each transfection, and the transfection efficiency was analyzed using a plasmid with enhanced green fluorescent protein marker. U937 and Kasumi-6 cells were transfected with nucleofection programmes V-01 and T-03, respectively. Transfection efficiencies of around 55–70% and 66–75% were observed in these cell lines, respectively.

Peptidyl–prolyl isomerase-parvulin inhibitor PiB (Calbiochem, Darmstadt, Germany) was prepared in ethanol and used at a concentration of 5 μM. C/EBPα small interfering RNA (siRNA) was purchased from Invitrogen.

Proteomics screening

To induce C/EBPα-p30, K562-C/EBPα-p30-ER cells were treated with 5 μM of β-estradiol for 6 h followed by lysis. The protein identification by mass spectrometry was carried out essentially, as reported before.[6]

Promoter assay

Cells (293T cells) were transiently transfected using lipofectamine (Invitrogen) as described by the manufacturer. Firefly luciferase activities from the PIN1 promoter constructs and *Renilla* luciferase activity from the internal control plasmid pRL-null were determined 24 h after transfection using the Dual-Luciferase Reporter Assay System (Promega, Mannheim, Germany). Firefly luciferase activities were normalized to the *Renilla* luciferase values of pRL-null.

Immunoblot analysis

Immunoblot analysis was performed with 50 μg total protein lysates using anti-C/EBPα (sc-61), anti-PIN1 (sc-15340), anti-c-Jun (sc-1694), anti-β-tubulin (sc-9104) and anti-E2F1 (sc-251) antibodies from Santa Cruz Biotechnology, Heidelberg, Germany. The immunodetection was performed using an ECL reagent (Amersham Biosciences, Freiburg, Germany). The band intensities were quantified using ImageJ software (National Institute of Health, Bethesda, MD, USA).

Chromatin immunoprecipitation

The crosslinking of proteins to DNA was accomplished by the addition of 1% formaldehyde for 10 min to cultured cells (6×10^6 cells) at 37 °C. After sonication, the chromatin was immunoprecipitated with 5 μg of the antibodies anti-E2F1 (sc-193X) or anti-IgG (SC-2027, Santa Cruz) at 4 °C overnight.

Flow cytometry analysis

For flow cytometry analysis, 10^6 cells were washed twice with phosphate-buffered saline and resuspended in 50 μl of phosphate-buffered saline with 2 μl of the respective antibody. Incubation was performed for 20 min in ice. After the incubation, cells were washed with phosphate-buffered saline, resuspended in phosphate-buffered saline and analyzed by flow cytometry on a FACScan (Becton Dickinson, Heidelberg, Germany).

mRNA expression analysis

Total RNA was isolated from leukemic patient samples, processed and analyzed on the Affymetrix HG-U133A and HG-U133B chips (Affymetrix, Santa Clara, CA, USA), as described before.[23] The data from Affymetrix analysis were normalized according to the procedure described before.[24] Normalized expression data were then analyzed with the R software package and the 'boxplot' function (www.r-project.org). Expression signal intensities are expressed on a logarithmic scale.

Real-time reverse transcription-PCR

Total RNA was isolated from cells with Trizol reagent (Invitrogen). RNA (750 ng) was used to synthesize cDNA by reverse transcription. Equal amounts of cDNA were taken for a subsequent quantitative real-time PCR using the SYBR Green PCR kit (Qiagen, Hilden, Germany) in a Rotor-Gene RG-3000 cycler (Corbett Research, Sydney, Australia). The fold change was calculated using delta C_T method reported before.[25]

Protein stability assay

Cells (293T cells) were transfected with 6.6 μg of PIN1 or nonsilencing siRNA (Qiagen) using lipofectamine. After 24 h, cells were treated with cyclohexamide (100 μg/ml) for various periods and lysed. The amount of c-Jun protein was analyzed by western blot and quantified by densitometric scanning.

Ubiquitination assay

Cells (293T cells) were transiently transfected with different constructs, as described for promoter assay; at 24 h after transfection, cells were lysed in radio immunoprecipitation assay buffer followed by c-Jun immunoprecipitation from 500 μg total protein. The protein samples after immunoprecipitation were analyzed in a 10% sodium dodecyl sulfate polyacrylamide gel electrophoresis gel and probed with an hemagglutinin antibody (Roche Applied Science, Mannheim, Germany).

Statistical analysis

We used Student's *t*-tests to determine the statistical significance of experimental results. A *P*-value of 0.05 or less was considered significant.

Results

C/EBPα-p30 induces PIN1 expression in leukemia

The K562-ER cell line is an early multipotential cell line derived from the K562 cell line, which was originally obtained from a patient with chronic myeloid leukemia. To derive the K562-ER cell line, K562 cells were stably transfected with a plasmid encoding an estrogen-inducible C/EBPα-p30 estrogen receptor fusion protein (C/EBPα-p30-ER).[21] K562-ER cells have been shown to be a good model system to study granulopoiesis in the context of C/EBPα proteins (Supplementary Figures 1 and 2). We have previously reported a proteomic approach for the identification of C/EBPα-p30 target proteins in C/EBPα-p30-ER cell line.[6] In this screen, PIN1 was identified as one of the targets of C/EBPα-p30 (Figure 1a).

As a first step to elucidate the importance and role of PIN1 as a target of C/EBPα-p30, we investigated the PIN1 mRNA levels in leukemic patient samples. Affymetrix analysis showed that PIN1 mRNA expression is increased in different subtypes of leukemia compared with normal bone marrow controls (Figure 1b). We also observed elevated PIN1 levels in AML samples with C/EBPα mutation in comparison with AML samples without C/EBPα mutation (Figure 1c). The increased expression of PIN1 in different leukemic subtypes suggests that mechanisms other than C/EBPα mutations can increase PIN1 levels (see Discussion). Next, we examined the ability of C/EBPα-p30 to induce PIN1 protein expression in the K562-C/EBPα-p30-ER cell line. Our data revealed that PIN1 protein expression was upregulated by C/EBPα-p30 during β-estradiol induction (Figure 1d left, Supplementary Figure 3). These data confirm our proteomic findings and reveal the relevance of PIN1 as a target in leukemia. We also investigated regulation of PIN1 during C/EBPα-p30 overexpression in two AML cell lines—Kasumi-6 (C/EBPα mutation positive) and NB4 (C/EBPα mutation negative). We observed that C/EBPα-p30 is able to upregulate PIN1 (Supplementary Figure 4). We observed slightly lower expression of PIN1 in Kasumi-6 cells in comparison with NB4 cells (Supplementary Figure 4). Similar to the upregulation of PIN1 protein levels, we observed an upregulation of PIN1 mRNA levels on C/EBPα-p30 induction (Supplementary Figure 5).

C/EBPα-p42 and C/EBPα-p30 have been shown to have different biological properties.[3] On the basis of our finding that C/EBPα-p30 is able to induce PIN1 expression, we asked whether C/EBPα-p42 is able to regulate PIN1 protein levels. Our data show that in contrast to the C/EBPα-p30 form, C/EBPα-p42 repressed PIN1 protein levels (Figure 1d, right). This shows that C/EBPα-p42 and C/EBPα-p30 have opposing effects on PIN1 protein levels. We could not find any regulation of PIN1 during C/EBPα-p42 silencing by siRNA (supplementary Figure 4). Hence, we assume that silencing of C/EBPα-p42 alone is not sufficient for the regulation of PIN1.

We also analyzed the role of C/EBPα with mutations in the E2F1 protein-binding domain (C/EBPα-BRM2)[21,26] in regulating PIN1 protein expression. Our data suggest that C/EBPα-BRM2 fails to downregulate PIN1 protein levels (data not shown). This denotes that E2F1 interaction of C/EBPα-p42 is necessary for its inhibitory action over PIN1.

C/EBPα-p30 induces PIN1 promoter activity in association with E2F1

It has been previously shown that there are three E2F1-binding sites in the PIN1 promoter and E2F1 can transactivate PIN1 promoter activity.[27] As we observed that C/EBPα-p30 induces PIN1 expression, we next investigated how C/EBPα proteins regulate PIN1 transcription. To address this, we performed promoter assays in the human embryonic kidney cell line 293T with different PIN1 promoter constructs.[27] Our data revealed that overexpression of E2F1 could transactivate PIN1 promoter, as published before (Figure 2a, compare bars 1 and 4). In comparison with E2F1 alone, cotransfection of C/EBPα-p30 enhanced the transactivation of the PIN1 promoter activity by approximately two folds (Figure 2a, compare bars 4 and 6). This indicates that C/EBPα-p30 cooperates with E2F1 to regulate PIN1 mRNA levels. Interestingly, cotransfection of C/EBPα-p42 downregulated PIN1 promoter activity (Figure 2a, compare bars 4 and 5).

To determine the importance of the three E2F1-binding sites for the C/EBPα-p30 cooperation with E2F1 in regulating PIN1 promoter activity, we performed promoter assays with different deletion mutants of PIN1 promoter (Figure 2b). Compared with the wild-type PIN1 promoter vector (−2300 Luc), deletion of the E2F1-binding sites (sites located at −557 to −550, −312 to −305 and at −288 to −281) exhibited decrease in the PIN1 promoter activity in a site-dependent manner (Figure 2c). These data suggest that E2F1-binding sites are important for the association of C/EBPα-p30 with E2F1.

To gain further insights into the mechanism of association of C/EBPα-p30 with E2F1 in regulating PIN1 expression, we performed chromatin immunoprecipitation assays in K562-C/EBPα-p30-ER cells. Cells were treated with β-estradiol to induce C/EBPα-p30 and chromatin fragments were immunoprecipitated with an anti-E2F1 antibody. DNA from the immunoprecipitates was PCR amplified using primers flanking the two E2F1-binding sites PIN1 promoter region shown in Figure 2d. We observed increased binding of E2F1 during C/EBPα-p30 induction in a time-dependent manner (Figure 2e). We analyzed whether increased binding of E2F1 in the PIN1 promoter is associated with induction of E2F1. Our data show that C/EBPα-p30 does not induce E2F1 protein (Supplementary Figure 6). It has been previously shown that C/EBPα-p30 is able to interact with E2F protein.[21] To evaluate whether interaction of C/EBPα-p30 with E2F1 has a role in the induction of PIN1 by C/EBPα-p30, we analyzed induction of PIN1 in a cell line that has mutation in the E2F1-interacting domain of C/EBPα-p30. Our data show that that E2F1 interaction is not needed for PIN1 induction (Supplementary Figure 7). Taken together, our data show that induction of C/EBPα-p30 leads to a recruitment of E2F1 to the PIN1 promoter and this is independent of interaction of C/EBPα-p30 with E2F1. These data suggest that PIN1 might represent an important target of E2F1 activation in the C/EBPα-p30-induced differentiation block. We also analyzed binding of C/EBPα-p30 to the PIN1 promoter in a similar experimental setting. We did not observe any binding of C/EBPα-p30 to the PIN1 promoter (data not shown).

To find the possibility of C/EBPα-p30 cooperation with E2F1 in regulating other E2F1 target genes, we performed chromatin immunoprecipitation in K562-C/EBPα-p30-ER cells for c-Myc promoter (Supplementary Figure 8). Even though we observed a slight increase in E2F1 binding in c-Myc promoter during C/EBPα-p30 induction, the effects were minor. This suggests that cooperation of C/EBPα-p30 with E2F1 is more effective in the regulation of PIN1 expression.